Cell

An archaic HLA class I receptor allele diversifies natural killer cell-driven immunity in First Nations peoples of Oceania

Graphical abstract

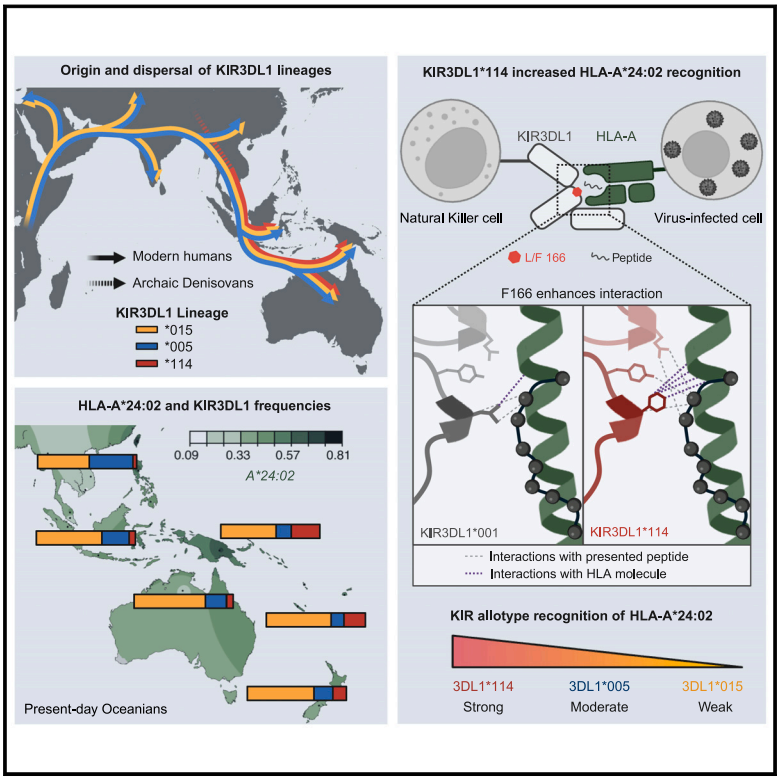

Highlights

- Archaic human natural killer (NK) cell receptor KIR3DL1 allele is frequent across Oceania
- Archaic KIR3DL1 has enhanced binding to modern human HLA class I ligand
- Enhanced binding allowed modern human ligand to expand in frequency
- Archaic admixture has lasting impact, modulating NK cell responses to infection

Authors

Liyen Loh, Philippa M. Saunders, Camilla Faoro, ..., Katherine Kedzierska, Andrew G. Brooks, Paul J. Norman

Correspondence

jamie.rossjohn@monash.edu (J.R.), steven.tong@unimelb.edu.au (S.Y.C.T.), kkedz@unimelb.edu.au (K.K.), agbrooks@unimelb.edu.au (A.G.B.), paul.norman@cuanschutz.edu (P.J.N.)

In brief

Predominant genetic variants found in First Nations peoples of the Oceania region influence the function of natural killer cells and may explain population-specific susceptibility to diseases, including influenza.

Loh et al., 2024, Cell *187*, 7008–7024
November 27, 2024
https://doi.org/10.1016/j.cell.2024.10.005

CellPress

CellPress
OPEN ACCESS

Cell

Article

An archaic HLA class I receptor allele diversifies natural killer cell-driven immunity in First Nations peoples of Oceania

Liyen Loh,[1,2,20] Philippa M. Saunders,[1,20] Camilla Faoro,[3,20] Neus Font-Porterias,[4,20] Neda Nemat-Gorgani,[5] Genelle F. Harrison,[4] Suraju Sadeeq,[4] Luca Hensen,[1] Shu Cheng Wong,[1] Jacqueline Widjaja,[1] E. Bridie Clemens,[1] Shiying Zhu,[3] Katherine M. Kichula,[4] Sudan Tao,[4,6] Faming Zhu,[6] Gonzalo Montero-Martin,[7] Marcelo Fernandez-Vina,[7] Lisbeth A. Guethlein,[5] Julian P. Vivian,[3] Jane Davies,[8,9] Alexander J. Mentzer,[10,11] Stephen J. Oppenheimer,[12] William Pomat,[13] Alexander G. Ioannidis,[14] Carmina Barberena-Jonas,[15] Oceanian Genome Variation Project Consortium, Andrés Moreno-Estrada,[15] Adrian Miller,[16] Peter Parham,[5] Jamie Rossjohn,[3,17,21,*] Steven Y.C. Tong,[18,19,21,*] Katherine Kedzierska,[1,21,*] Andrew G. Brooks,[1,21,*] and Paul J. Norman[2,4,5,21,22,*]

[1]Department of Microbiology and Immunology, University of Melbourne at the Peter Doherty Institute for Infection and Immunity, Melbourne, VIC 3000, Australia
[2]Department of Immunology and Microbiology, University of Colorado School of Medicine, Aurora, CO 80045, USA
[3]Infection and Immunity Program and Department of Biochemistry and Molecular Biology, Biomedicine Discovery Institute, Monash University, Clayton, VIC 3800, Australia
[4]Department of Biomedical Informatics, University of Colorado School of Medicine, Aurora, CO 80045, USA
[5]Department of Structural Biology and Department of Microbiology and Immunology, Stanford University, Stanford, CA 94305, USA
[6]Blood Center of Zhejiang Province, Hangzhou, Zhejiang, China
[7]Stanford Blood Centre, Department of Pathology, Stanford University, Stanford, CA 94305, USA
[8]Menzies School of Health Research, Charles Darwin University, Darwin, NT 0810, Australia
[9]Department of Infectious Diseases, Royal Darwin Hospital, Casuarina, NT 0810, Australia
[10]Wellcome Centre for Human Genetics, University of Oxford, Oxford OX3 7BN, UK
[11]Big Data Institute, Li Ka Shing Centre for Health Information and Discovery, University of Oxford, Oxford OX3 7LF, UK
[12]Institute of Social and Cultural Anthropology, School of Anthropology and Museum Ethnography, University of Oxford, Oxford OX3 7LF, UK
[13]Papua New Guinea Institute of Medical Research, Post Office Box 60, Goroka, Papua New Guinea
[14]Department of Biomolecular Engineering, UC Santa Cruz, Santa Cruz, CA 95064, USA
[15]Advanced Genomics Unit, Center for Research and Advanced Studies (CINVESTAV), Irapuato 36821, Mexico
[16]Jawun Research Centre, Central Queensland University, Cairns, QLD 4870, Australia
[17]Institute of Infection and Immunity, Cardiff University School of Medicine, Heath Park, Cardiff CF14 4XN, UK
[18]Victorian Infectious Diseases Service, The Royal Melbourne Hospital, Peter Doherty Institute for Infection and Immunity, University of Melbourne, Parkville, VIC 3000, Australia
[19]Department of Infectious Diseases, Peter Doherty Institute for Infection and Immunity, University of Melbourne, Parkville, VIC 3000, Australia
[20]These authors contributed equally
[21]These authors contributed equally
[22]Lead contact
*Correspondence: jamie.rossjohn@monash.edu (J.R.), steven.tong@unimelb.edu.au (S.Y.C.T.), kkedz@unimelb.edu.au (K.K.), agbrooks@unimelb.edu.au (A.G.B.), paul.norman@cuanschutz.edu (P.J.N.)
https://doi.org/10.1016/j.cell.2024.10.005

SUMMARY

Genetic variation in host immunity impacts the disproportionate burden of infectious diseases that can be experienced by First Nations peoples. Polymorphic human leukocyte antigen (HLA) class I and killer cell immunoglobulin-like receptors (KIRs) are key regulators of natural killer (NK) cells, which mediate early infection control. How this variation impacts their responses across populations is unclear. We show that HLA-A*24:02 became the dominant ligand for inhibitory KIR3DL1 in First Nations peoples across Oceania, through positive natural selection. We identify KIR3DL1*114, widespread across and unique to Oceania, as an allele lineage derived from archaic humans. KIR3DL1*114^{+}NK cells from First Nations Australian donors are inhibited through binding HLA-A*24:02. The KIR3DL1*114 lineage is defined by phenylalanine at residue 166. Structural and binding studies show phenylalanine 166 forms multiple unique contacts with HLA-peptide complexes, increasing both affinity and specificity. Accordingly, assessing immunogenetic variation and the functional implications for immunity are fundamental toward understanding population-based disease associations.

INTRODUCTION

Host genetics influences immune responses, contributing to the disproportionate morbidity and mortality from infectious diseases experienced by First Nations peoples.[1–4] During viral infection, HLA class I displays peptides derived from virus proteins on the surface of infected cells, rendering them liable for elimination by cytotoxic cells of immunity. Extensive HLA-A, -B, and -C polymorphisms both define the repertoire of peptides that may be presented by a given individual and impact immune cell receptor binding.[5,6] For example, whereas HLA-A*02:01 and -B*08:01, which are HLA class I types frequent in populations of European genetic ancestry, mediate protection from severe influenza disease, HLA-A*24:02, which is highly prevalent in First Nations Oceanian and American populations, associates with poor outcome.[7] Although HLA-A*02:01, A*24:02, and B*08:01 all mediate strong influenza-specific cytotoxic T cell responses,[8–10] only A*24:02 is also a ligand for inhibitory KIR3DL1, expressed by natural killer (NK) cells.[11] NK cells act early in immune responses by killing infected cells, releasing cytokines, and stimulating adaptive immunity.[12] Interaction of inhibitory killer cell immunoglobulin-like receptor (KIR) with HLA class I prevents NK cells from destroying healthy cells while enabling them to sense any virus-induced HLA class I downregulation.[13–15] Importantly, the ability to respond to missing or altered HLA in this manner is defined by inherited combinations of the highly polymorphic *HLA class I* and *KIR* genes.[16]

Not every individual has all the KIR capable of interacting with HLA class I, and not every HLA class I allele can form a KIR ligand.[17] This genetically established combinatorial diversity distinguishes individuals in their infection outcomes.[18] In addition to modulating effector functions, signaling through KIR educates developing NK cells to recognize the specific HLA class I ligands expressed by a given individual.[19] The strength of inhibitory signal transduction, which is dependent both on KIR and HLA allotype, calibrates the effector and killing capacity of the mature NK cells.[20,21] Among polymorphic receptors shaping diversity of NK cell responses to viral infection, inhibitory KIR3DL1 dominates.[22,23] Enabling recognition by KIR3DL1, HLA-A*24:02 carries the "Bw4" sequence motif, occurring in amino acid residues 77–83, and common to a subset of HLA-A and -B allotypes.[24] There are two ancient lineages of KIR3DL1, which are the 015 lineage that interacts poorly with HLA-A*24, favoring HLA-B allotypes, and the 005 lineage that interacts both with HLA-A and -B allotypes.[25,26] Although there is a predominance of $Bw4^+$ HLA-A allotypes across Oceania, there is also a relative lack of 005-lineage KIR3DL1.[27]

Likely following emigration out of Africa, present-day First Nations Oceanians diverged from Eurasians ~50–70 kya.[28,29] Subsequent admixture with archaic humans introduced new genetic material, having major impact on genes of the immune system.[30–36] Archaic human refers to the extinct hominins, such as Denisovans, who diverged from modern humans in Africa ~600,000 years ago to populate Europe and Asia.[37] We examined the immunogenetic composition of First Nations Oceanians and identified a unique and divergent form of KIR3DL1 having characteristics of archaic human sequence. Because such archaic introgression rarely involves protein-coding variation, favoring regulatory elements,[38,39] we investigated the origin, distribution, and functions of this allele to determine if it could impact the course of NK cell-driven immunity across Oceania.

RESULTS

High combinatorial diversity of HLA and KIR in First Nations Australians

Reflecting differential genetic ancestries, environments, and pathogen exposures, human populations have accumulated characteristic *HLA* allele spectra.[40] In 80 First Nations Australians from northern Australia,[7] we identified 18, 33, and 25 alleles of HLA-A, -B, and -C, respectively (Table S1). Accounting for sample size, this observed diversity in *HLA class I* alleles is similar to Europeans and West Africans, representing an intermediate between First Nations Papua New Guineans and southern Africans (Nama and Khomani: Figure 1A), who are among the most genetically diverse humans.[42] A haplotype refers to a specific combination of alleles that are inherited together. The *HLA class I* alleles form 79 distinct haplotypes in the First Nations Australian cohort (Table S1). The most frequent alleles for each locus, *HLA-A*34:01* (24%), *-B*13:01* (18%), and *-C*04:01* (23%), respectively, comprise the most frequent *HLA class I* haplotype (Figure 1B). *HLA-A*34:01* and *-B*13:01* are characteristic to Oceanian populations,[43,44] and analysis of genome-wide SNPs shows this haplotype is Australian/Oceanian in origin (Figures 1B and S1). Seven of the ten most frequent *HLA class I* haplotypes have similar Oceanian-related ancestry, whereas three are of likely European descent (Figure 1B).

Together, the 76 unique HLA class I alleles encode 67 distinct protein sequences (allotypes) in First Nations Australians (Figure 1C). Bw4 is the motif that forms the ligand for KIR3DL1 carried by some HLA-A and -B allotypes (ligands and nomenclature are described in STAR Methods). In First Nations Australians, HLA-A*24:02 is the most frequent $Bw4^+$ HLA allotype present (21.9%) followed by B*15:22, B*44:02, and B*44:03 (each 2.5%, Table S1). These HLA allotypes bind more strongly to 005 lineage than to 015-lineage KIR3DL1 allotypes.[23,26] Thus, in First Nations Australians, most $Bw4^+$ HLA will interact preferentially with 005-lineage KIR3DL1, and in other Oceanians, all the $Bw4^+$ HLA will interact preferentially with 005-lineage KIR (Figure 1D).

KIR polymorphism affects the capacity of NK cells to respond to infection-induced changes in HLA class I expression.[18,45,46] Of the 13 *KIR* genes, a total of 121 alleles were identified in the cohort, including 27 first characterized here (Figure 1E; Table S1). In addition to KIR3DL1, other KIRs differentially bind A3 and A11, or the C1 or C2 motifs of HLA class I (STAR Methods). In the cohort of First Nations Australians, KIR2DL1 (specific for $C2^+$HLA) has nine allotypes, 2DL2/3 (specific for C1 and some C2) has eight, 3DL1 (Bw4) has 13, and 3DL2 (A3/11) has eleven (Figure 1F). The inhibitory KIR alleles are arranged in 55 distinct haplotypes (Figure 1G; Table S1), and every individual in the cohort has a unique combination of KIR and ligands (Figure 1H). The distribution of *KIR* and *HLA class I* alleles is characteristic of a diverse population, due in part to admixture with Europeans, in accordance with genome-wide data.[28] First Nations Australians from northern Australia represent a population with substantial genetic variation that has the potential to diversify the NK cell response to viral infections.[13]

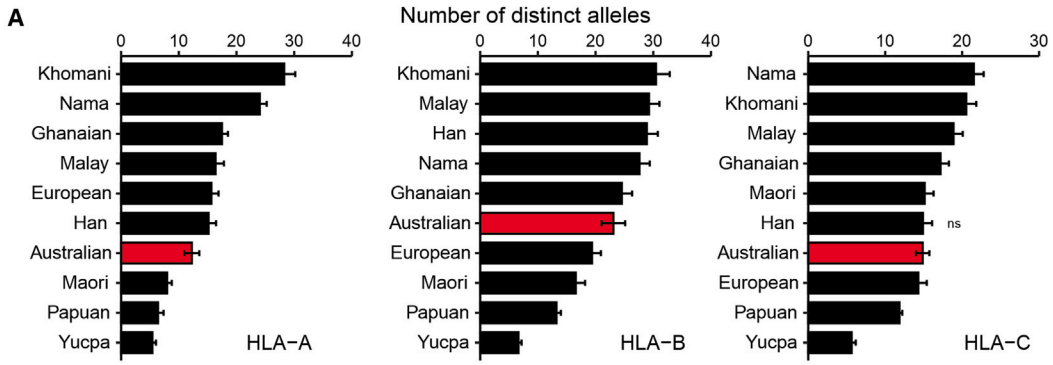

B

	HLA class I haplotype A	B	C	AUS	PNG	EUR	EAS	
1	*34:01:01	*13:01:01	*04:01:01					
2	*02:01:01	*07:02:01	*07:02:01					†
3	*24:02:01	*40:01:02	*03:03:01					
4	*34:01:01	*56:01:01	*01:02:01					
5	*34:01:01	*15:21	*04:03:01					
6	*24:02:01	*13:01:01	*04:01:01					
7	*01:01:01	*08:01:01	*07:01:01					†
8	*11:01:01	*15:21	*04:03:01					
9	*24:02:01	*56:01:01	*01:02:01					
10	*01:01:01	*57:01:01	*06:02:01					†

KIR ligand: A3/11, Bw4, No KIR motif, C1, C2
Freq (%): 0 4 8 12

C

	Allotypes	N.	Freq (%)	Distribution
HLA-A	Total	18		
	A3/11	2	18.7	
	Bw4	3	24.3	
HLA-B	Total	31		
	Bw4	8	12.5	
HLA-C	Total	18		
	C1	11	50.6	
	C2	7	49.4	

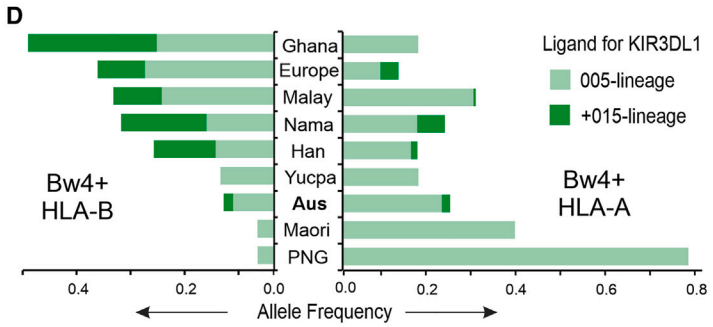

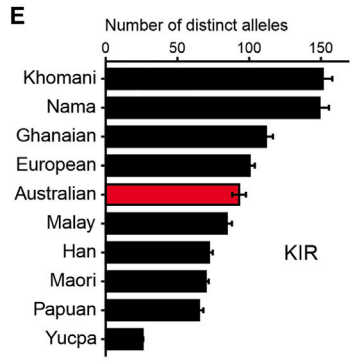

F

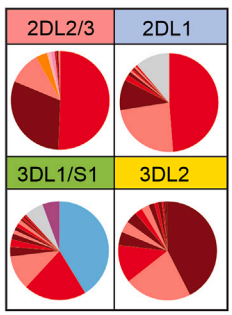

G

2DL2/3	2DL1	3DL1	3DL2	freq.
3*001	*003		*007	0.210
3*001	*003	*015	*002	0.143
2*001	*004		*007	0.112
2*001			*007	0.043
3*002	*002		*007	0.034
2*001	*004	*005	*010	0.029
3*001	*003	*005	*010	0.026
2*001	*004	*015	*002	0.026
3*001	*003	*114	*070	0.025
2*001		*005	*010	0.017

H

Distinct Genotypes	N (/80)
HLA class I	80
KIR	77
KIR + ligand	80

(legend on next page)

The First Nations KIR3DL1*114 allotype is divergent and likely introgressed

KIR3DL1 is encoded by the *KIR3DL1/S1* locus, which also encodes the activating KIR3DS1, differentiating an additional lineage.[47] All three lineages of KIR3DL1/S1 were observed in First Nations Australians, with the 005 lineage represented by three cell-surface expressed allotypes, the 015 lineage by six allotypes, and 3DS1 by a single allotype (Figure 2A). All five *KIR3DL1* alleles we first identified here encode distinct allotypes (Table S1). Of these, *KIR3DL1*114* was observed in five of the 80 individuals. The KIR3DL1*114 protein sequence is distinguished from KIR3DL1*015 by three and *005 by five amino acid changes (Figure 2B). Importantly, KIR3DL1*114 possesses phenylalanine at position 166. Residue 166 is subject to positive natural selection for diversity in hominids,[47] with three alternative residues found at this site in humans (Figure 2B). Residue 166 is located in the second Ig domain (D1) at the interface with the HLA-peptide complex.[24,48]

The residues alanine 88 and phenylalanine 166 (Phe-166) that characterize KIR3DL1*114 are shared with KIR3DL1*086, previously identified in Māori[27] (Figure 2B). To determine the wider distribution of these alleles, we analyzed genome-wide SNP data for 1,210 unrelated Oceanians, comprising 913 samples from the Oceanian Genomic Variation Project (OGVP),[49] and an additional 297 Papua New Guinean individuals.[50] We also sequenced the *KIR* and *HLA* genes from an overlapping cohort of 645 Papuans. Examining their global distribution (STAR Methods) indicates *KIR3DL1*086* and **114* are both specific to Oceanians (Figure 2C). Conservative estimates of the allele frequencies range from 1% in Kinh Vietnamese to 21% in Lowland and 28% in Highland Papuans (Table S3). From individuals having both sequence and SNP data, we inferred the local genetic ancestry and identified 54/56 (92.9%) *KIR3DL*114*$^{+}$ haplotypes as Papuan, with a positive correlation of *KIR3DL1*114* with Papuan-related ancestry across Oceania and Southeast Asia (Figures S2A–S2D). Thus, *KIR3DL1*114* is characteristic to and widespread throughout Oceania and likely shared by gene flow into southeast Asia.

Throughout Oceania, *KIR3DL1*114* and **086* are each observed in tight linkage with *KIR2DL4*028* and *KIR2DS4*019* (Figure 2D), which, together with *KIR3DL2*070*, characterize the First Nations Australian *KIR3DL1*114*$^{+}$ haplotypes (Figure 2D). Each of the four alleles is distinguished from the closest known allele[51] by at least two unique single nucleotide substitutions. Analysis of *HLA* genotypes confirmed the five individuals are unlikely to be first- or second-degree relatives. Intrigued by the distinct characteristics and established evidence that archaic admixture is detectible in Oceanians,[52,53] we further investigated *KIR3DL1*114* carrying haplotypes. Indeed, the D-statistic, which determines allele sharing across lineages,[33,54] shows statistically significant evidence that the *KIR3DL1*114* haplotype has an allele composition shared with the Denisovan genome (D score = 0.95, Z score = 40.6, Figure 2E). This analysis also showed the minimum length of the haplotype to be 62,276 bp (Table S3), spanning the *KIR2DL4* through *KIR3DL2* genes. We estimate *KIR3DL1*114* diverged from the KIR3DL1 015- and 005-lineages 1.84 mya (95% CI: 0.994–2.996, STAR Methods). This divergence time is older than the split between archaic and modern humans, and the **114* allele group is absent from Africa, suggesting re-introduction from archaic humans to Oceanian ancestors.[32] A competing hypothesis is the ancestral lineage present in both modern and archaic humans was lost from Africa either during or shortly after the out-of-Africa migration. However, the probability of a haplotype of 62.3 kbp being shared by modern Oceanians and Denisovans due to incomplete ancestral lineage sorting is extremely low (8.78×10^{-9}),[55] further supporting transfer to modern humans from archaic humans. The geographical distribution and sequence divergence of *KIR3DL1*114* carrying haplotypes and significant allele sharing with Denisovan therefore make them clear candidates for originating from archaic hominins through introgression.[32,35]

HLA-A*24:02 is the dominant ligand for KIR3DL1 in First Nations Australians (Figure 1), and the mean allele frequency of *A*24:02* across Oceania and Southeast Asia is 46.1% ± 19.6% (Figure 2C; Table S3). HLA is subject to balancing selection, favoring heterozygotes, and promoting diversity in defense against pathogens.[56–58] By contrast here, homozygosity of *HLA-A* is higher than expected under neutrality, as indicated by the Ewens-Watterson F-statistic (e.g., $p < 0.05$ in Australia; Table S3). In Australia and Papua New Guinea, HLA-A*24:02 drives the reduced *HLA-A* diversity, where the number of *A*24:02* homozygotes is significantly higher than expected

Figure 1. High combinatorial diversity of HLA and KIR in First Nations Australians

(A) Shown is the number of distinct *HLA-A*, *-B*, and *-C* alleles of 75 random individuals for each indicated population. Error bars represent mean ± standard deviation from 1,000 resamples with replacement. Unpaired two-sample Wilcoxon tests with Bonferroni multiple test correction were performed between First Nations Australians (shaded red) and each reference population (p for each comparison is <0.001, except with Han for HLA-C, which is not significant, ns).

(B) The ten most frequent *HLA class I* haplotypes detected in First Nations Australians. The KIR ligands are colored: A3/11 (yellow), Bw4 (green), C1 (red), and C2 (blue). At the right are shown their frequencies in First Nations Australians (AUS), Papua New Guineans (PNG), Europeans (EUR), and East Asians (EAS) (key is underneath). †, haplotype of likely European origin (Figure S1; Table S2).

(C) The distribution of KIR ligands among HLA class I allotypes. The combined frequencies of each subset are shown.

(D) Shows the total allele frequencies of Bw4^{+} HLA-B (left) and Bw4^{+} HLA-A (right) across the representative populations. Bw4^{+} allotypes that preferentially interact with 005 lineage KIR3DL1 are shown in light green; those that interact with 005 and 015 lineage in dark green.

(E) The number of distinct *KIR* alleles detected in 75 individuals from each of the populations indicated, obtained as described for (A).

(F) Frequency spectra of *KIR* alleles encoding inhibitory receptors specific for HLA class I (colored by cognate ligand from B). Each segment corresponds to a distinct KIR allotype. (Blue) Activating KIR3DS1, (purple) allotypes that are not expressed on the cell surface,[41] and (gray) gene absence.

(G) Ten most frequent haplotypes considering inhibitory KIR specific for HLA class I.

(H) The number of distinct *HLA class I* and *KIR* genotypes observed in 80 First Nations Australians. "KIR + ligand" excludes non-expressed allotypes and non-functional interactions.

An explanation of HLA and KIR nomenclature is given in STAR Methods.

See also Figure S1.

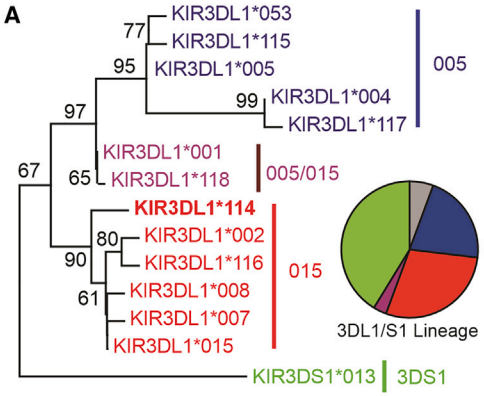

B

KIR3DL1/S1 allotype	Domain	D0							D1				D2	
	Residue	2	20	47	54	58	88	92	138	163	**166**	182	199	283
	L1*015	V	R	V	L	S	P	V	G	P	**L**	P	P	W
	L1*114	M	-	-	-	-	A	-	-	-	**F**	-	-	-
	L1*086	M	Q	I	I	-	A	-	-	-	**F**	-	-	-
	L1*005	M	-	I	I	-	-	-	-	-	**-**	S	-	L
	S1*013	M	-	-	I	G	-	M	W	S	**R**	-	L	-

C

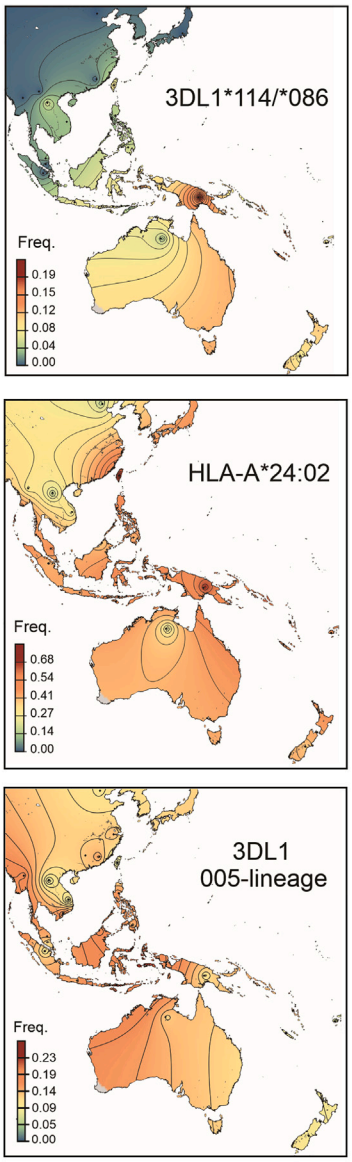

D

Origin	*2DL4*	*3DL1/S1*	*2DS4*	*3DL2*	N
First Nations Australian (2N=160)	*028	*114	*019	*070	4
	*028	*114	*019	*002	1
Vietnamese (2N=248)	*028	*114	*019	*070	2
Malay (2N=184)	*028	*114	*019	*101	2
	*028	*114	*019	*002	1
Māori (2N=98)	*028	*086	n.d.	*002	4
Polynesian (2N=68)	*028	*086	n.d.	*002	4
Papua New Guinean (2N=1,290)	*028	*114	*019	*002	334
	*028	*086	*019	*002	18
	*028	*114	*019	*111	7
	*028	*114	*019	*070	4
	*028	*114	*019	*010	1

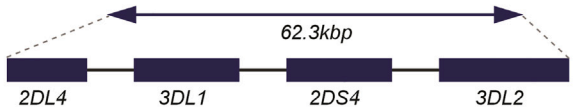

E

W	D	Z
*114	0.95	40.6
*005	0.39	1.75
*015	-0.52	-2.46

F

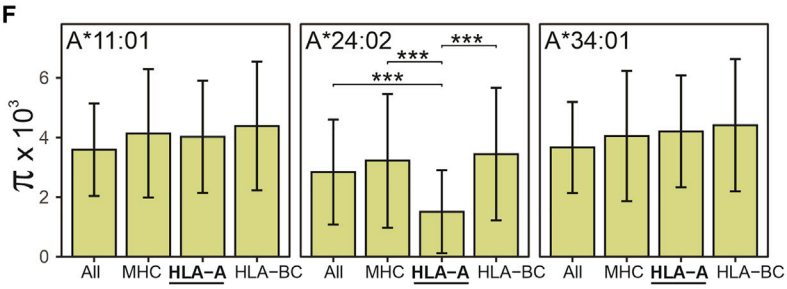

G

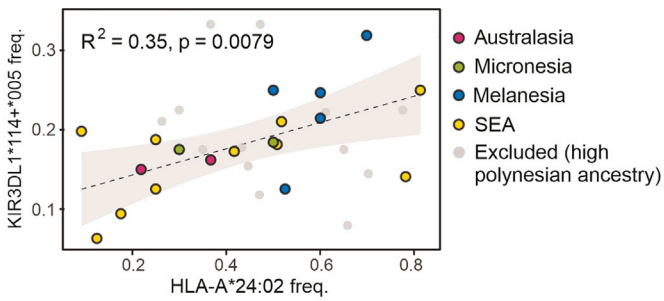

(legend on next page)

under Hardy-Weinberg equilibrium ($p < 0.05$, Table S3). The reduced genetic diversity of *HLA-A*24:02* is not observed in the rest of the genome or in other *HLA-A* alleles (Figure 2F; Table S3), and we found no evidence that *HLA-A*24:02* has archaic human origin (Figure S2E). An earlier study suggested high frequency of HLA-A*24:02 is due to positive natural selection.[59] Here, we used the iHS test, which can detect positive selection within 1,000 generations of present, and identified a signal acutely centered on *HLA-A*24:02* (Figure S2F).

Finally, although we observed the high frequency of HLA-A*24:02 does not correspond with the frequency of 3DL1*005, its strongest-binding KIR partner (Figure 2C), we did observe a statistically significant positive correlation of *HLA-A*24:02* with the combined allele frequencies of *KIR3DL1*005* and **114* (Figure 2G). These findings suggest that the rapid frequency rise of HLA-A*24:02 across Oceania was permitted by the presence of KIR3DL1*114 compensating for the scarcity of KIR3DL1*005-lineage allotypes.

KIR3DL1*114 has 005 lineage properties

KIR3DL1 polymorphism can determine cell surface expression level, which can impact NK cell function.[47] With exceptions, 015 lineage allotypes are expressed at high levels on the NK cell surface, and 005 lineage at low levels.[47] To determine the cell-surface expression of KIR3DL1*114, we analyzed NK cells isolated from blood donors selected according to their *KIR3DL1/S1* genotype (Figures S3A and S3B). KIR3DL1*114 is expressed on the NK cell surface at significantly lower levels than KIR3DL1*015 or *001 allotypes ($p = 0.0007$ and $p = 0.0013$, respectively) and at a similar level to KIR3DL1*005 (Figure 3A). Thus, the expression level of this allotype is like the 005 lineage.

By measuring upregulation of CD107a and interferon (IFN)-γ, we tested the response of primary NK cells to target cells expressing HLA-A*24:02. Whereas all KIR3DL1$^+$ NK cells responded to HLA-deficient targets, NK cells expressing KIR3DL1*114 or *005 were more inhibited by HLA-A*24:02 than those expressing KIR3DL1*001 or *015-like allotypes (Figure 3B). Showing that the inhibition is specific to KIR3DL1, the response was not significantly diminished in NK cells expressing only KIR2DL2/3 or KIR2DL1 from the same donors, assessed in parallel (Figure 3C). To determine NK cell responses against a broader set of target cells transfected with HLA class I, we used interleukin-2 (IL-2)-expanded KIR3DL1$^+$ NK cells from donors expressing KIR3DL1*001, *005, *015, or *114 (Table S4). The targets included all three Bw4$^+$ HLA-A and six of eight Bw4$^+$HLA-B allotypes identified in the First Nations Australian cohort (Figure 3D). Also included were B*27:05, which preferentially binds KIR3DL1*005, and A*25:01, which does not bind KIR3DL1.[11,26] All four KIR3DL1 allotypes strongly inhibited NK cells from killing target cells expressing HLA-A*32:01, B*44:02, B*51:01, or B*57:01 (Figure 3D). Against the remaining targets, we observed a functional hierarchy, with KIR3DL1*015 and *001 mediating the least, *005 the greatest, and *114 an intermediate degree of NK cell inhibition (Figure 3D). Within this hierarchy, NK cells expressing KIR3DL1*114 resemble those expressing KIR3DL1*001 and *015 in their lack of response to HLA-B*13:01 and B*27:04/06 targets, yet resemble those expressing KIR3DL1*005 in being inhibited by HLA-A*23:01 and A*24:02 (A*23:01 is closely related to A*24:02, sharing identity in Bw4 motif and surrounding residues[51]). The observed differences of KIR3DL1*114$^+$NK cell activities are statistically significant (two-way ANOVA; $p < 0.05$–$p < 0.001$; Figure 3D). The ligand specificity of KIR3DL1*114 is thus distinct from other allotypes tested in being broader than 015 lineage and narrower than 005-lineage allotypes.

Phenylalanine at residue 166 of KIR3DL1 enhances recognition of HLA-A*24:02

To test the hypothesis that Phe-166 determines the specificity of KIR3DL1*114, we performed *in vitro* analyses using reporter cells expressing extracellular domains of individual KIR3DL1 allotypes (Figures S3D–S3F). Here, KIR3DL1*114 reporter cells responded less strongly to HLA-B*51:01 expressing targets than those expressing 3DL1*001, *005, or *015, but had enhanced response toward HLA-B*57:01 targets ($p < 0.01$–0.001; Figure 3E). Whereas KIR3DL1*005 and *114 reacted strongly to HLA-A*24:02 and B*27:05 targets, KIR3DL1*001 and *015 did not ($p < 0.001$; Figure 3E). We thus observed the same hierarchy of KIR3DL1 allotype strength as observed using IL-2-expanded NK cells (Figure 3D). Mutating residue 166 of KIR3DL1*015 (Figure 3F) from leucine to phenylalanine significantly increased activity toward HLA-A*24:02, B*27:05, and B*57:01 ($p < 0.01$–0.001) but had no effect on the recognition of HLA-B*13:01 or B*27:06-expressing

Figure 2. KIR3DL1*114 has archaic human origin and coevolved with HLA-A*24:02 in Oceania

(A) Neighbor-joining phylogenetic analyses of external-domain coding sequences of the KIR3DL1/S1 allotypes observed in First Nations Australians. Colors represent the three major KIR3DL1/S1 lineages, 005 (blue), 015 (red), 3DS1 (green), and recombinant 005/015 alleles (purple). KIR3DL1*114 clusters in the 015 lineage. Bootstrap values for nodes are given when >50%. Lower right pie chart shows relative allele frequencies of the three lineages, according to the same color scheme, and gray indicates gene absence.

(B) Polymorphic amino acid residues distinguishing the lineages of KIR3DL1/S1, alongside KIR3DL1*086 and *114. KIR3DL1*015 is used as the reference sequence; residues identical to *015 are indicated by dashes. Residue 166 is shown in bold.

(C) Geographic distribution of *KIR3DL1*114/*086*, *HLA-A*24:02*, and *KIR3DL1 005*-lineage alleles in Oceania and Southeast Asia (Table S3).

(D) *KIR* haplotypes carrying *KIR3DL1*114* or **086* and the populations from where they were characterized. (n.d., not determined).

(E) D-statistics for testing Denisovan introgression of *KIR3DL1*114* ($n = 4$), **005* ($n = 6$), and **015* ($n = 6$). KIR3DL1*114 only includes homozygous individuals. W, haplotypes contain indicated allele; *Z*, *Z* score; D, D score. See STAR Methods and Table S3.

(F) Nucleotide diversity (π) across distinct regions of the genome in *HLA-A*24:02*, *HLA-A*34:01*, and *HLA-A*11:01* homozygous Papua New Guineans. π in 100 bp windows; *HLA-A* and *-BC* are flanking 500 kbp on each side. (***$p < 0.001$, compared with *HLA-A*; Wilcoxon test; Table S3). Error bars represent mean ± standard deviation.

(G) Correlation of *HLA-A*24:02* with *KIR3DL1*114+005-lineage* allele frequencies. Each dot represents a population, colored by region (SEA, Southeast Asia). Only populations with less than 50% Polynesian-related ancestry (by RFMix) are included (others are shown in gray).

See also Figure S2.

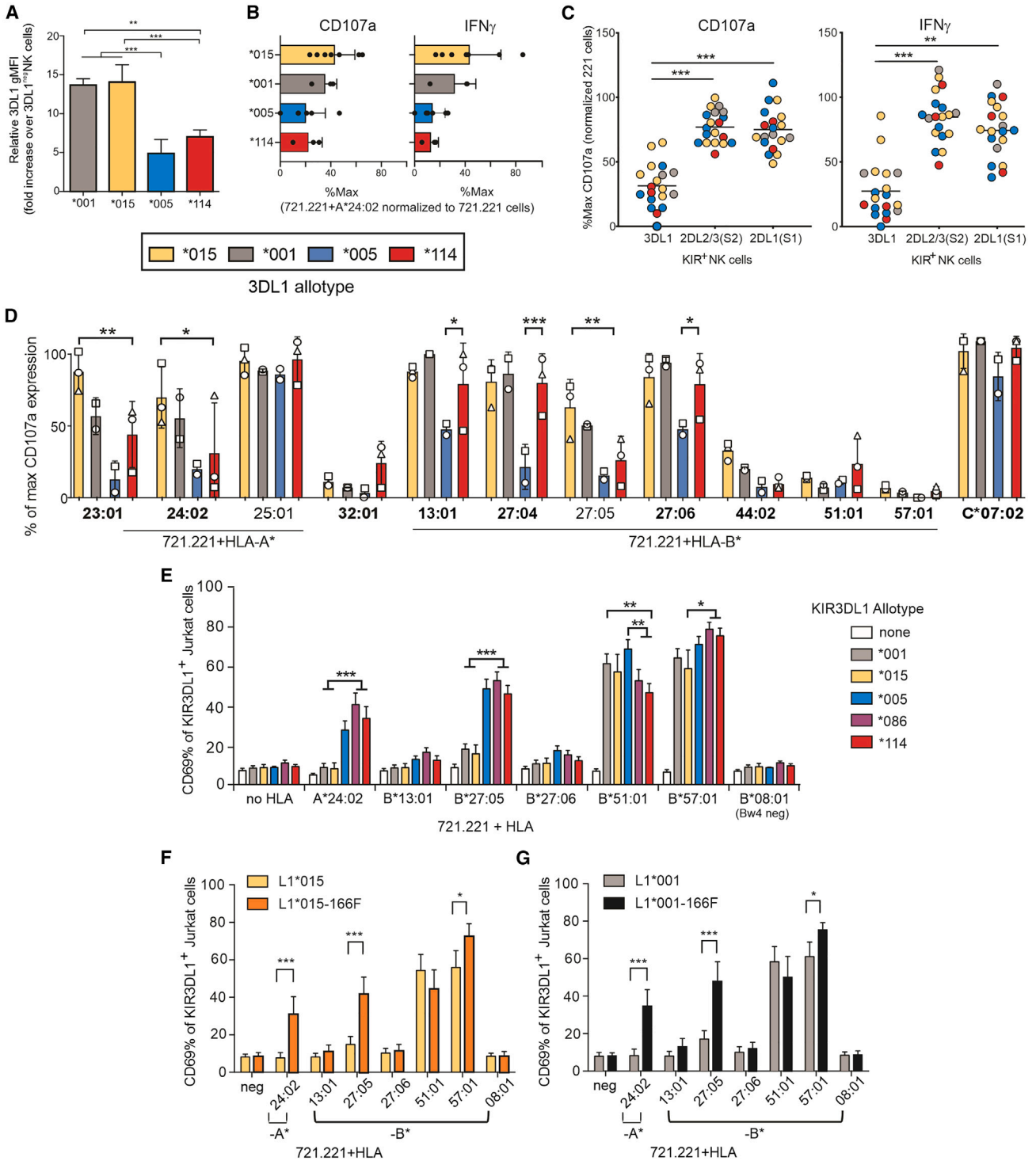

Figure 3. KIR3DL1*114 inhibits NK cells upon recognition of HLA-A*24:02

(A) Shows KIR3DL1 expression levels on the cell surface of primary NK cells isolated from individuals having KIR3DL1*114 ($n = 3$), *001 ($n = 3$), *005 ($n = 4$), or *015-lineage ($n = 4$) allotypes (Figures S3A and S3B; Table S4). The geometric mean fluorescence intensity (gMFI) of KIR3DL1 expression for each allotype was normalized within each donor to KIR3DL1^{neg} NK cells. $^{**}p < 0.01$, $^{***}p < 0.001$; Kruskal-Wallis test. Error bars indicate the standard deviation of the mean.

(B) Shows CD107a (left) and IFN-γ (right) expression by *ex vivo* NK cells following incubation with 721.221 cells expressing HLA-A*24:02. NK cells were isolated from donors expressing KIR3DL1*114 ($n = 3$), *001 ($n = 3$), *005 ($n = 6$), or *015-like ($n = 7$). For each donor, values are normalized (% max) to those obtained from

(legend continued on next page)

targets. In these experiments, KIR3DL1*086 had the same recognition pattern as *114 (Figure 3E), which was recapitulated through leucine to phenylalanine substitution of KIR3DL1*001 residue 166 (Figure 3G). Together, these results clearly show the distinct functional profile observed for KIR3DL1*114^{+}NK cells isolated from First Nations Australian donors is due to Phe-166.

To understand how substitution at residue 166 affects receptor function, we compared crystal structures of KIR3DL1*001 and KIR3DL1*114, each bound to HLA-A*24:02 complexed with the TW9 peptide. TW9 comprises influenza A virus polymerase basic protein 2, residues 549–557, and induces a CD8^{+}T cell response when presented by HLA-A*24:02.[60] We determined the structures to 1.9 Å and 2.4 Å resolution, respectively (Table S5). Whereas the overall docking geometry of these two KIR3DL1-HLA receptor-ligand complexes[24,48] remains conserved (Figure 4A), KIR3DL1*001 and *114 differ in their interactions both with the Bw4 motif and the presented peptide (Figures 4B and 4C). Namely, leucine 166 (Leu-166) forms one van der Waals (vdw) interaction with isoleucine 80 of the Bw4 motif, whereas Phe-166 forms nine vdw contacts, interacting with residues 76 and 80 of HLA (Figure S4). The extensive network of hydrophobic contacts with Bw4 thus enhances recognition of the HLA class I molecule by KIR3DL1*114 (Figure 4B). Likewise, KIR3DL1*114 directly contacts residues 7 and 8 of the TW9 peptide (P7 and P8) through three hydrogen bonds and three vdw interactions, whereas KIR3DL1*001 makes only two vdw contacts and no hydrogen bonds with P8 (Figure S4). Thus, KIR3DL1*114 makes more extensive contacts with HLA-A*24:02-TW9 in comparison to KIR3DL1*001.

Included in the peptide contacts made by KIR3DL1*114 are tyrosine 200 (Tyr-200) and glutamic acid 282 (Glu-282), which interact with P8, and P7 and P8 of the peptide, respectively. By comparison, in the KIR3DL1*001-HLA-A*24:02-peptide complex, P8-Asparagine is rotated away from the interface, preventing the formation of hydrogen bonds with Glu-282 and Tyr-200 of KIR3DL1*001 (Figure 4C). Concomitant with the altered orientation of P8, Glu-282 adopts a different conformation compared with the same residue in KIR3DL1*114, increasing the distance from P7 to ~5 Å, precluding the formation of a direct contact between these two residues (Figure 4C). These findings show how Phe-166 enhances interaction with ligand both through direct and indirect mechanisms. Crystallographic analysis of further receptor-ligand complexes with HLA class I presenting two other distinct epitopes (a viral and a self-peptide) showed this enhancement is observed across disparate ligands for KIR3DL1*114 (Figure 4D; Table S5). Similar results were obtained for KIR3DL1*086, which also carries Phe-166 (Figure 4D). Here, the strongest expected interactions are Phe-166^{+}KIR3DL1 with HLA-A*24:02-NEF (HIV peptide) and with B*57:03-AW10 (self-peptide), having four and twelve vdw contacts with peptide, respectively (Figure S4). In summary, polymorphism at residue 166 has a substantive role in determining the functional specificity of KIR3DL1.

KIR3DL1*114 strongly binds influenza peptides presented by HLA-A*24:02

Given that position 166 of KIR3DL1 affects ligand specificity and contacts the HLA-bound peptide, we investigated the peptide specificity of this polymorphism. We selected three influenza A virus peptides known to bind HLA-A*24:02[60] (Figures 5A and S5) and examined their binding to *001, *015, *005, *086, and *114 allotypes of KIR3DL1. We also selected one HIV and one self-derived peptide, known to bind KIR3DL1 when in complex with HLA-A*24:02 or B*57:03, respectively.[61,62] In surface plasmon resonance (SPR) experiments, all five HLA class I-peptide complexes bound to each of the KIR3DL1 allotypes (Figure S5). For each given ligand, we observed a clear hierarchy of binding. The KIR3DL1 allotypes showed their greatest distinction in affinity for HLA-B*57:03-AW10 (Figure 5B), where KIR3DL1*001, *005, and *015 bound weakly with a K_D of 40–60 μM, and KIR3DL1*086 and *114 binding affinities were 20- to 30-fold stronger, having a K_D of 2 μM (Figure S5). This notable increase in affinity is consistent with the crystallography data showing multiple interactions with the ligand complex mediated specifically by Phe-166 (Figure 4; Table S5). Although the binding hierarchy was the same with HLA-A*24:02-TW9, KIR3DL1*005 represented an intermediate between the two extremes of low-affinity KIR3DL1*001 or *015, and high-affinity KIR3DL1*086 or *114 (Figure 5C). To confirm the impact of Phe-166, we made KIR3DL1*086-166L and *114-166L constructs and repeated the SPR experiments. Both 3DL1*086-166L and *114–166L showed reduced binding affinities for the HLA-peptide complexes, in each case being like those of KIR3DL1*005

KIR3DL1^{+} NK cells incubated with the parental, HLA class I^{neg} 721.221 cell line. Each dot represents one donor. CD107a $p = 0.07$, IFN-γ $p = 0.02$; Kruskal-Wallis test.

(C) As (B), except NK cells were differentiated into those expressing only KIR3DL1, KIR2DL1/S1, or KIR2DL2/3/S2. Each circle represents one donor. Responses were normalized to the maximal obtained with the parental 221 cell line and compared using a one-way ANOVA with Tukey's multiple comparison test (**$p < 0.01$, ***$p < 0.001$).

(D) Assays using NK cells isolated from ten donors and expanded *in vitro* using IL-2. Each donor was homozygous for one of four expressed KIR3DL1 allotypes. HLA allotype of target cells is indicated on the x axis (allotypes present in the cohort shown in bold). CD107a expression of KIR3DL1^{+} NK cells was normalized to the maximal expression in response to parental 721.221 cells. Background CD107a expression by NK cells was subtracted. For each donor, two-three replicates were performed, and the mean of all replicates from the donors is shown as the bar graph with the standard deviation plotted. ***$p < 0.001$, **$p < 0.01$, *$p < 0.05$; two-way ANOVA with Bonferroni's multiple comparisons. For each KIR3DL1 allotype, triangles, circles, and squares represent the donors used, whose genotypes are given in Table S4.

(E–G) Shows the result of *in vitro* activation (CD69 upregulation) of reporter cells expressing specific KIR3DL1 allotypes. Jurkat cells were transduced with a given natural (E) or mutated (F and G) KIR3DL1 allotype that was fused to the intracellular domain of CD3ζ. Colors represent the KIR3DL1 allotypes, as shown in the key. The reporter cells were incubated with a panel of 721.221 target cells for 8 h, and the subsequent upregulation of CD69 was assessed by flow cytometry (Figures S3D and S3E). Three independent experiments were performed, each in triplicate, and statistics performed on the average of the replicates. *$p < 0.05$, **$p < 0.001$, ***$p < 0.001$; two-way ANOVA with Tukey's multiple comparisons test.

See also Figure S3.

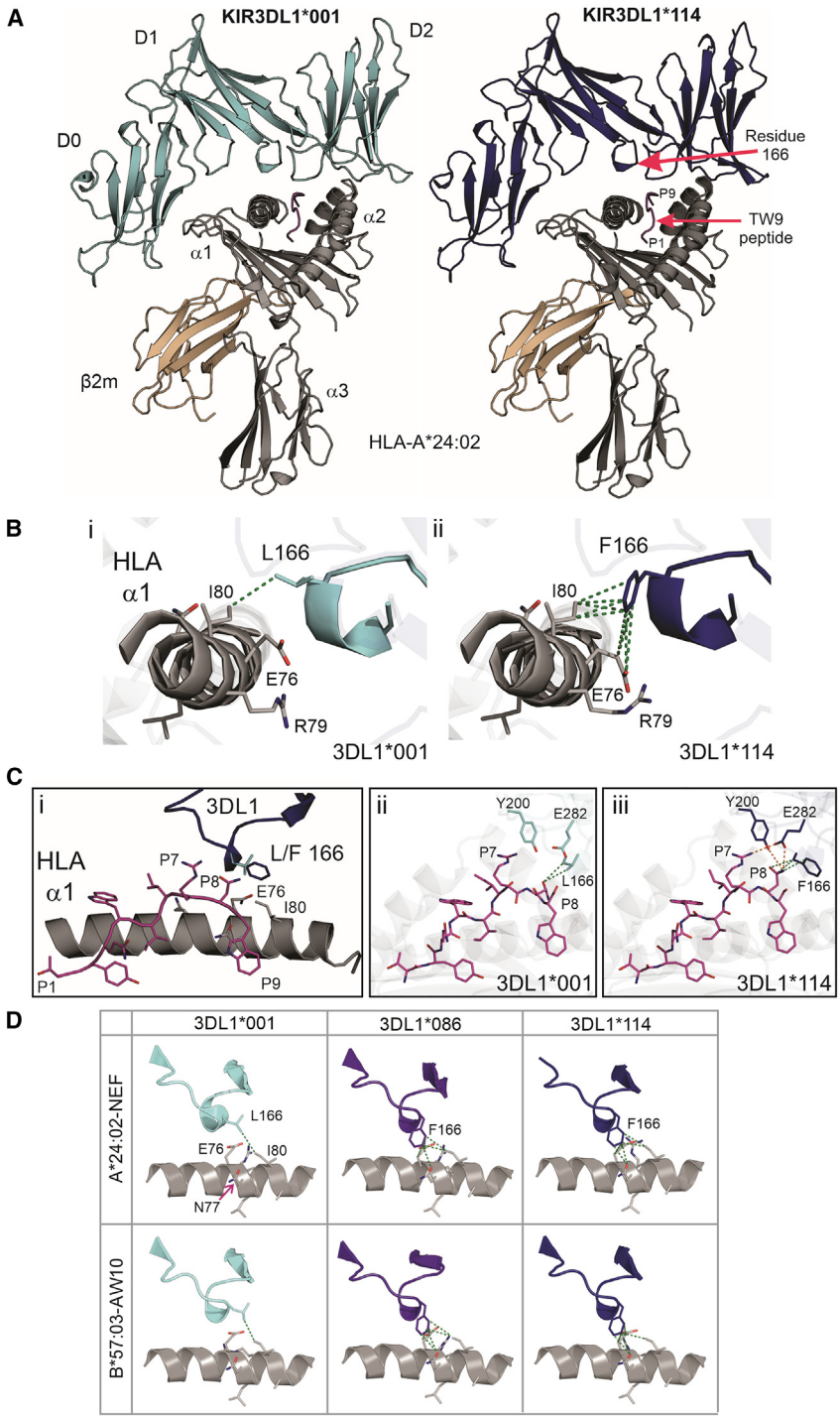

Figure 4. Phenylalanine at residue 166 of KIR3DL1*114 enhances interaction with HLA ligands

(A) Ribbon diagram of the crystal structures solved for KIR3DL1*001 (left, cyan) and KIR3DL1*114 (right, blue) bound to the HLA-A*24:02-TW9 peptide (influenza virus A polymerase basic protein 2 residues 549–557) complex. HLA-A*24:02 in gray, peptide in mauve, and β_2M in orange. KIR3DL1 and HLA domains are labeled on the left, and positions of the peptide and residue 166 are indicated on the right.

(B) Orthogonal view of KIR3DL1 residue 166 interactions with α1 helix residues of the HLA molecule. (Bi) KIR3DL1*001 (L166), (Bii) KIR3DL1*114 (F166). Dotted lines indicate van der Waals interactions.

(C) (Ci) Side view; cut away to show the interactions of KIR3DL1 residue 166 with peptide and HLA molecules. Leucine 166 is represented shaded cyan and phenylalanine dark blue. (Cii) Aerial view of peptide showing contacts with L166 and (Ciii) F166.

(D) Comparison of interactions of KIR3DL1 residue 166 from allotypes (left to right) KIR3DL1*001, *086, and *114 with HLA α1 helix residues of (top) HLA-A*24:02-NEF and (bottom) -B*57:03-AW10. NEF is derived from HIV-1, AW10 from human catenin.

See also Figure S4.

(Figures 5B and 5C). The exception was HLA-A*24:02-FF10, which had similar affinity for each of the KIR3DL1 allotypes tested (Figures S5C and S5D).

Overall, the binding profiles of KIR3DL1*086 and *114 showed statistically significant higher affinity values for HLA-A*24:02 complexes than did KIR3DL1*001 or *015 (Figures 5D and 5E). The greatest variety in binding was seen for KIR3DL1*005, which bound to HLA-A*24:02-NEF and B*57:03-AW10, with similar affinity as KIR3DL1*001 and *015, to HLA-A*24:02-FF10 with similar affinity as KIR3DL1*086 and *114, and to the remainder at intermediate affinity (Figure S5). Interestingly, FF10 has the same sequence as RF8, but with two additional residues at the N terminus (Figure 5A). These residues increased the affinity for all KIR3DL1 allotypes, most noticeably for KIR3DL1*005, placing this allotype with similar or greater affinity for the FF10 peptide as KIR3DL1*086 and *114 (Figure 5D). Together, these results suggest that 005-lineage allotypes of KIR3DL1 are highly peptide selective. They also indicate that Phe-166 enhances interaction with HLA-A*24:02 while reducing the sensitivity of KIR3DL1 for the presented peptide.

DISCUSSION

Combinatorial diversity of KIR and HLA class I modulates NK cell-driven control of infectious disease severity.[63,64] Through killing infected cells, NK cells act before, during, and after development of a memory immune response. Having roles also in conventional T cell-driven immunity, NK cells can lyse specific antigen-presenting cells or kill infected cells through antibody-dependent cytotoxicity (ADCC), and KIR can modulate potentially autoreactive T cells.[65–68] Optimal interaction of KIR with HLA can therefore

A

HLA	Peptide	Sequence										Origin
		1	2	3	4	5	6	7	8	**9**	10	
A*24:02	$TW9_{549-557}$		T	Y	Q	W	I	I	R	**N**	W	
	$RF8_{498-505}$			R	Y	G	F	V	A	**N**	F	IAV
	$FF10_{496-505}$	F	Y	R	Y	G	F	V	A	**N**	F	
	$NEF_{134-141}$			R	Y	P	L	T	F	**G**	W	HIV-1
B*57:03	$AW10_{850-859}$	A	S	L	N	L	P	A	V	**S**	W	Human

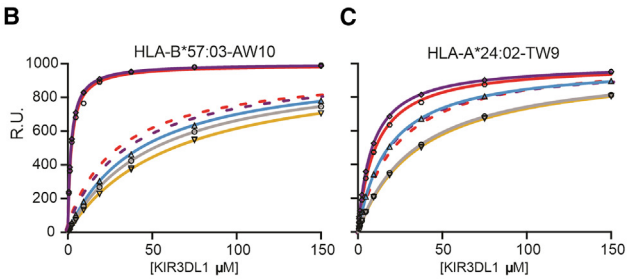

mean K_D	*001	*015	*005	*086	*086-F166L	*114	*114-F166L
B*57:03 AW10	50.87	62.36	42.9	1.99	35.72	2.07	31.37
A*24:02 TW9	34.65	36.61	18.07	8.88	18.97	10.44	20.06

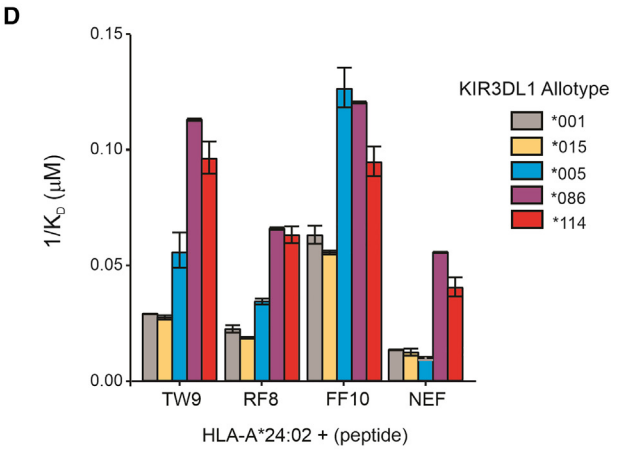

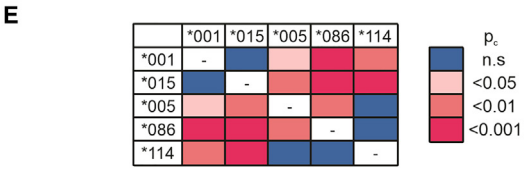

Figure 5. KIR3DL1 allotypes having phenylalanine at residue 166 bind HLA-A*24:02-peptide complexes with greater affinity than do other allotypes

(A) (Left to right) HLA class I allotype, and name, sequence, and origin of bound peptide. Residues in bold correspond to P8 of the 9-mer peptide.

(B and C) Shown are the affinity curves of soluble KIR3DL1 allotypes binding to the immobilized HLA-B*57:03-AW10 (B) or HLA-A*24:02-TW9 complex (C). The KIR3DL1 allotypes are *001, *005, *015, *086, and *114, and mutations *086-F166L, *114-F166L. R.U., response units. Mean from two independent experiments shown. Underneath are shown the mean K_D values; ± values and remaining HLA-A*24:02-peptide binding curves are given in Figure S5.

(D) Comparison of K_D values across HLA-A*24:02-peptide complexes. Data are representative of two independent experiments. Error bars are SEM.

determine whether an infection is controlled without incurring collateral damage, both in the short and long term. Consequently, genetically determined diversity of KIR and HLA class I affects the severity of multiple immune-mediated diseases and may also affect the course of specific immunotherapies, including transplantation.[16] Among the KIR/HLA interactions, those of the inhibitory KIR3DL1 with subtypes of HLA-A or -B dominate in diversity and known implications for infectious disease. KIR3DL1 alleles are highly differentiated across populations,[25] likely influencing control of region-specific infections.[69] We identified KIR3DL1*114 to have strong affinity for HLA-A*24:02 and their pairing to be uniquely common across Oceania. KIR3DL1 allotypes that bind most strongly to their ligands drive generation of the most potently acting NK cells. In autoimmunity and some viral infections, the strongly inhibiting KIR3DL1 allotypes can associate with protection from disease severity.[16,70,71] By contrast, in hematopoietic cell transplantation for acute myeloid leukemia, where donor NK cells can kill host leukemic cells, strongly inhibiting KIR3DL1 allotypes associate with leukemic relapse.[72] Moreover, these strongly inhibiting allotypes may also reduce success of monoclonal antibody therapy for specific tumors,[73] but improve the course of checkpoint inhibition therapy for others.[74] However, most of the above findings have been established for individuals of European descent, and little is known about the extent or implications of immunogenetic variation in First Nations peoples. Our precise functional characterization of the allotypes we describe here therefore has potential application for multiple aspects of human health across the Oceania region.

We identified *KIR3DL1*114* as an ancient allele group unique to Oceania that is likely introgressed from Denisovans. Having a mean allele frequency of 8.5% across Oceania and 25% in Papua New Guinea, we estimate a minimum of 5 million people to have KIR3DL1*114. The polymorphism that defines the specificity of KIR3DL1*114 occurs at a site previously identified under natural selection for diversity.[25] We show HLA-A*24:02, the contemporary ligand for KIR3DL1*114, rose to high frequency across Oceania under positive selection during the time since KIR3DL1*114 was acquired by modern humans. Together, these findings suggest the presence of KIR3DL1*114 permitted HLA-A*24:02 to rise in frequency and that the interaction of this HLA-A with *114 compensates for the lack both of Bw4 motifs carried by HLA-B and the 005 lineage of KIR3DL1. Although the cause and timing of the selection are unknown, one outcome is a unique profile of NK cell receptor diversity for modern-day individuals in this geographic region, defined by a predominance of strongly inhibitory KIR3DL1 specific for HLA-A. Having distinct evolutionary histories,[13] HLA-A and -B likely complement each other in function. Although we did not directly study the impact of KIR3DL1*114 on NK cell education, strong interaction of KIR3DL1*114 with HLA-A*24:02 implicates this combination as a robust educator of NK cells. Any implications for host immunity of NK cells preferentially interacting with HLA-A remain to be established.

(E) Comparison of K_D values obtained by the KIR3DL1 allotypes across the four HLA-A*24:02 complexes. t test, Bonferroni corrected (Pc).

See also Figure S5.

Although not selected by any health criteria, the initial cohort was assembled to investigate the high prevalence of severe influenza disease in First Nations Australians.[4,7] Influenza virus remains a major threat to human health,[75] and treatment for severe disease is limited. One of the most frequent HLA class I allotypes in the cohort and the most frequent across Oceania is A*24:02, which presents a risk for developing severe respiratory disease following influenza infection.[10] Peak influenza virus replication occurs within days of infection, prior to the establishment of T cell-driven immune responses. Subsequently, memory T cells ensure repeat challenges by the same or similar virus strain are eliminated. Innate immune responses are therefore necessary to ensure survival when challenged by a strain not previously encountered. NK cells are critical in this early response.[76,77] NK cells can recognize and kill influenza-infected cells,[78] and NK cell activation is critical for coordinating and modulating cytotoxic T cell activity to influenza virus infection.[79] Further highlighting the importance of their role fighting this infection, influenza virus has evolved multiple strategies to evade NK cells.[80] Accordingly, impaired NK cell function associates with influenza virus susceptibility.[81] Potentially impairing their function, NK cells isolated from lungs express high levels of inhibitory KIR,[67] and influenza virus infection causes redistribution of HLA class I on the cell surface such that KIR binds more efficiently.[82] That HLA-A*24:02, uniquely among HLA class I allotypes common in Oceania, enables interaction with KIR3DL1 implicates NK cells in the increased susceptibility to severe influenza observed for First Nations Oceanians.

Resembling the functional characteristics of the KIR3DL1*114 interaction with HLA-A*24:02, KIR2DL1 is a stronger and more specific receptor for HLA-C than is KIR2DL3.[83] In individuals carrying both KIR2DL1 and KIR2DL3, those NK cells expressing KIR2DL1 had a more inhibited response to influenza-virus-infected cells than those expressing KIR2DL3.[84] Although the effects of KIR3DL1 polymorphism were not investigated, those findings suggest that the strong specific inhibition of NK cells mediated by KIR3DL1*114 interaction with HLA-A*24:02 will be detrimental to control of influenza virus infection. The influenza virus peptides we studied here had been selected for their ability to stimulate cytotoxic T cell activity when complexed with HLA-A*24:02,[60] yet we show the same complexes strongly and specifically inhibit NK cell effector activities. Strong inhibition of NK cells may limit their ability to control influenza virus infection. Alternatively, any reduced ability of NK cells to dampen the T cell-driven immune responses may increase the likelihood for collateral damage.[15] The implications of these findings will therefore need further investigation in severe influenza disease settings.

Previous work identifying introgressed immune genes identified single molecules of limited, albeit critical, function in innate immunity and have tended to identify non-coding variants that may affect expression.[30,39] Exceptions include one rare (HLA-B*73) and one more frequent (HLA-A*11) HLA allele but with no data regarding their functions obtained.[35] By contrast, we describe an immune receptor allotype characteristic to Oceania and currently representing up to 30% individuals in populations throughout this geographic region. The interaction of NK cell receptors with HLA has wide-ranging implications for innate and adaptive immunity, not limited to infectious disease, including autoimmunity, cancer, immunotherapy, and neurological disease. As we present direct evidence for functional distinction of the interactions involving KIR3DL1*114, our work thus shows how archaic admixture could have lasting impact on the health of First Nations peoples. We also note that, in addition to archaic introgression, we show that more recent gene flow from Europeans has had a substantial impact on the immunogenetic diversity of First Nations Australians in relation to other First Nations Oceanians.

Limitations of the study

Phe-166 is encoded by a CTT-TTT codon change carried by a haplotype that we show to be highly likely of Denisovan origin. All haplotypes sharing flanking SNPs from the 369 that we sequenced also carried the TTT codon. Although we assume from this observation that Phe-166 is Denisovan in origin, it cannot be ruled out from the data we have that any of the SNPs that define this haplotype could have been derived in modern humans since the Denisovan admixture event took place.

Population-specific co-evolution of KIR and HLA class I ligands is a defining feature of the KIR/HLA class I system.[85] Here, the prevailing dogma is that the system is subject to balancing selection, whereby populations respond rapidly to any perturbations of the balance through polymorphism that alters specificity or function.[16] KIRs appear to be evolving more rapidly than HLA, able to alter function through single nucleotide substitution, gene deletion, duplication, or fusion, and here we also highlight the use of pre-existing variation.[86] Although we have focused the study on infectious diseases, combinatorial diversity of KIR and HLA class I may be affected by natural selection through their critical role early in placentation.[13,16] As HLA-A and -B are not expressed by fetal trophoblast cells, the role of NK cells in reproduction is unlikely to have driven the co-evolution of KIR3DL1*114 with HLA-A*24:02. An assumption we therefore make is that the combination of HLA-A*24:02 with KIR3DL1*114 has been advantageous toward controlling specific pathogen or pathogens that remain unknown. Further work is therefore required to identify the pathogens and whether they remain a threat to health in Oceania.

RESOURCE AVAILABILITY

Lead contact

Further information and requests for the resources should be directed to and will be fulfilled by the lead contact, Dr. Paul J. Norman (paul.norman@cuanschutz.edu).

Materials availability

The reagents generated in this study will be made available upon reasonable request to the lead contact.

Data and code availability

- De-identified human HLA and KIR locus-specific raw sequence data have been deposited in the Harvard Dataverse as https://doi.org/10.7910/DVN/TRMTCT and https://doi.org/10.7910/DVN/JA0U1Z. As of the date of publication, they are available upon request to lead contact, if access is granted.

- Sequences of the newly characterized HLA and KIR alleles have been deposited in GenBank under accession numbers MH301276-78 and MH938271-297 and are publicly available as of the date of publication.
- Protein structures were deposited in the Research Collaboratory for Structural Bioinformatics Protein Data Bank under accession codes, 9BL2-6, 9BL9, and 9BLA, and are publicly available as of the date of publication.
- This paper does not report any original code.
- This paper analyzes existing, publicly available data, accessible at PDB: 7K80, https://www.ebi.ac.uk/ipd/, https://ftp.ncbi.nlm.nih.gov/pub/mhc/mhc/Final%20Archive/IHWG/Anthropology/, https://www.internationalgenome.org/, https://www.simonsfoundation.org/simons-genome-diversity-project/.
- Any additional information required to analyze the data reported in this paper is available from the lead contact upon request.

CONSORTIA

The members of the Oceanian Genome Variation Project are George Aho, Angela Allen, Stephen Allen, Kathryn Auckland, Andreia Brandao, Ram Gonzalez Buenfil, Carlos D. Bustamante, Phillip Endicott, Francoise Friedlaender, Jonathan S. Friedlaender, Adrian V.S. Hill, Julian R. Homburger, Alexander G. Ioannidis, Carmina Barberena Jonas, Toomas Kivisild, George Koki, Alexander J. Mentzer, Andrés Moreno-Estrada, Stephen Oppenheimer, Tom Parks, Maude Phipps, William Pomat, Eliuel Pretrick, Consuelo D. Quinto-Cortés, Martin Richards, Kathryn Robson, Jean Roux, Sofía Vieyra Sánchez, Alissa L. Severson, Pedro Soares, Abdul Salam M. Sofro, Matthew Spriggs, Mark Stoneking, Tamarua Teariki, Ishwar Verma, Joyce White, and Genevieve L. Wojcik.

ACKNOWLEDGMENTS

We thank all the First Nations participants for taking part in this study. This work was supported by ARC DP190103282 (K.K., A.G.B., and L.L.), NHMRC GNT1042662 (K.K., S.Y.C.T., and A.M.), NHMRC GNT1122524 (K.K., S.Y.C.T., and A.M.), NHMRC GNT1145033 (S.Y.C.T.), NIH R01 AI17892 (P.P.), and NIH R01 AI151549 (P.J.N.). K.K. is supported by an NHMRC Leadership Investigator Fellowship (#1173871), J.R. by an NHMRC Leadership Investigator Fellowship, and J.P.V. by a Victorian Cancer Agency fellowship. E.B.C. is supported by an NHMRC Peter Doherty Fellowship (#1091516). We acknowledge the Melbourne Cytometry Platform (Doherty Institute node) for the provision of flow cytometric services. We acknowledge the University of Colorado Barbara Davis Center for Sanger sequencing (NIH P30 DK116073).

AUTHOR CONTRIBUTIONS

Conceptualization, A.G.B., K.K., S.Y.C.T., A.M., and P.J.N.; investigation, L.L., P.M.S., C.F., N.N.-G., L.H., S.C.W., J.W., S.Z., G.M.-M., K.M.K., E.B.C., L.A.G., and P.J.N.; formal analysis, L.L., P.M.S., C.F., N.F.-P., G.F.H., S.T., S.S., J.P.V., and P.J.N.; resources, S.Y.C.T., J.D., A.M., P.P., M.F.-V., F.Z., A.J.M., S.J.O., W.P., A.G.I., C.B.-J., A.M.-E., P.J.N., J.R., K.K., and A.G.B.; funding acquisition, K.K., A.G.B., L.L., P.J.N., J.R., P.P., S.Y.C.T., and A.M.; writing – original draft, L.L., P.M.S., C.F., N.F.-P., P.P., J.R., K.K., A.G.B., and P.J.N.; writing – review and editing, all authors.

DECLARATION OF INTERESTS

A.G.I. has shares in Galatea Bio, Inc. G.F.H. is currently an employee of Tempus AI. S.C.W. is currently an employee of Miltenyi Biotec Asia Pacific Pte Ltd. L.H. is affiliated with the Department of Internal Medicine II, University Hospital Tübingen, Tübingen, Germany. J.W. is affiliated with The Malignant Hematology, Transplantation, and Cellular Therapy Services, Alfred Health, Melbourne, VIC, Australia. S.Z. is affiliated with the Protein Production Facility (PPF) of the Walter and Eliza Hall Institute of Medical Research, Melbourne, VIC, Australia. G.M.-M. is affiliated with the HLA Histocompatibility and Immunogenetics Laboratory, Vitalant, Phoenix, AZ, USA. J.P.V. is affiliated with St. Vincent's Institute of Medical Research, Fitzroy, VIC, Australia.

STAR★METHODS

Detailed methods are provided in the online version of this paper and include the following:

SUPPLEMENTAL INFORMATION

Supplemental information can be found online at https://doi.org/10.1016/j.cell.2024.10.005.

Received: June 19, 2023
Revised: May 24, 2024
Accepted: October 3, 2024
Published: October 29, 2024

REFERENCES

1. Keynan, Y., Malik, S., and Fowke, K.R. (2013). The role of polymorphisms in host immune genes in determining the severity of respiratory illness caused by pandemic H1N1 influenza. Public Health Genomics *16*, 9–16. https://doi.org/10.1159/000345937.
2. Tarantola, A., Horwood, P., Richard, V., and Quintana-Murci, L. (2018). Host and viral genetic diversity can help explain mortality during the 1918–21 influenza pandemic in the Pacific region. Lancet Infect. Dis. *18*, 833–834. https://doi.org/10.1016/S1473-3099(18)30408-0.
3. La Ruche, G., Tarantola, A., Barboza, P., Vaillant, L., Gueguen, J., and Gastellu-Etchegorry, M.; Epidemic Intelligence Team at InVS (2009). The 2009 pandemic H1N1 influenza and indigenous populations of the Americas and the Pacific. Euro Surveill. *14*, 19366. https://doi.org/10.2807/ese.14.42.19366-en.
4. Flint, S.M., Davis, J.S., Su, J.Y., Oliver-Landry, E.P., Rogers, B.A., Goldstein, A., Thomas, J.H., Parameswaran, U., Bigham, C., Freeman, K., et al. (2010). Disproportionate impact of pandemic (H1N1) 2009 influenza on Indigenous people in the Top End of Australia's Northern Territory. Med. J. Aust. *192*, 617–622.
5. Dendrou, C.A., Petersen, J., Rossjohn, J., and Fugger, L. (2018). HLA variation and disease. Nat. Rev. Immunol. *18*, 325–339. https://doi.org/10.1038/nri.2017.143.

6. Trowsdale, J., and Knight, J.C. (2013). Major histocompatibility complex genomics and human disease. Annu. Rev. Genomics Hum. Genet. *14*, 301–323. https://doi.org/10.1146/annurev-genom-091212-153455.

7. Clemens, E.B., Grant, E.J., Wang, Z., Gras, S., Tipping, P., Rossjohn, J., Miller, A., Tong, S.Y.C., and Kedzierska, K. (2017). Towards identification of immune and genetic correlates of severe influenza disease in Indigenous Australians. Immunol. Cell Biol. *95*, 648. https://doi.org/10.1038/icb.2017.47.

8. Moss, P.A., Moots, R.J., Rosenberg, W.M., Rowland-Jones, S.J., Bodmer, H.C., McMichael, A.J., and Bell, J.I. (1991). Extensive conservation of alpha and beta chains of the human T-cell antigen receptor recognizing HLA-A2 and influenza A matrix peptide. Proc. Natl. Acad. Sci. USA *88*, 8987–8990. https://doi.org/10.1073/pnas.88.20.8987.

9. Quiñones-Parra, S., Grant, E., Loh, L., Nguyen, T.H.O., Campbell, K.A., Tong, S.Y.C., Miller, A., Doherty, P.C., Vijaykrishna, D., Rossjohn, J., et al. (2014). Preexisting CD8+ T-cell immunity to the H7N9 influenza A virus varies across ethnicities. Proc. Natl. Acad. Sci. USA *111*, 1049–1054. https://doi.org/10.1073/pnas.1322229111.

10. Hertz, T., Oshansky, C.M., Roddam, P.L., DeVincenzo, J.P., Caniza, M.A., Jojic, N., Mallal, S., Phillips, E., James, I., Halloran, M.E., et al. (2013). HLA targeting efficiency correlates with human T-cell response magnitude and with mortality from influenza A infection. Proc. Natl. Acad. Sci. USA *110*, 13492–13497. https://doi.org/10.1073/pnas.1221555110.

11. Stern, M., Ruggeri, L., Capanni, M., Mancusi, A., and Velardi, A. (2008). Human leukocyte antigens A23, A24, and A32 but not A25 are ligands for KIR3DL1. Blood *112*, 708–710. https://doi.org/10.1182/blood-2008-02-137521.

12. Lam, V.C., and Lanier, L.L. (2017). NK cells in host responses to viral infections. Curr. Opin. Immunol. *44*, 43–51. https://doi.org/10.1016/j.coi.2016.11.003.

13. Parham, P., and Moffett, A. (2013). Variable NK cell receptors and their MHC class I ligands in immunity, reproduction and human evolution. Nat. Rev. Immunol. *13*, 133–144. https://doi.org/10.1038/nri3370.

14. Björkström, N.K., Strunz, B., and Ljunggren, H.G. (2022). Natural killer cells in antiviral immunity. Nat. Rev. Immunol. *22*, 112–123. https://doi.org/10.1038/s41577-021-00558-3.

15. Mahmoud, A.B., Tu, M.M., Wight, A., Zein, H.S., Rahim, M.M.A., Lee, S.H., Sekhon, H.S., Brown, E.G., and Makrigiannis, A.P. (2016). Influenza virus targets Class I MHC-educated NK cells for immunoevasion. PLoS Pathog. *12*, e1005446. https://doi.org/10.1371/journal.ppat.1005446.

16. Pollock, N.R., Harrison, G.F., and Norman, P.J. (2022). Immunogenomics of killer cell immunoglobulin-like receptor (KIR) and HLA Class I: coevolution and consequences for human health. J. Allergy Clin. Immunol. Pract. *10*, 1763–1775. https://doi.org/10.1016/j.jaip.2022.04.036.

17. Uhrberg, M., Valiante, N.M., Shum, B.P., Shilling, H.G., Lienert-Weidenbach, K., Corliss, B., Tyan, D., Lanier, L.L., and Parham, P. (1997). Human diversity in killer cell inhibitory receptor genes. Immunity *7*, 753–763. https://doi.org/10.1016/S1074-7613(00)80394-5.

18. Martin, M.P., Naranbhai, V., Shea, P.R., Qi, Y., Ramsuran, V., Vince, N., Gao, X., Thomas, R., Brumme, Z.L., Carlson, J.M., et al. (2018). Killer cell immunoglobulin-like receptor 3DL1 variation modifies HLA-B*57 protection against HIV-1. J. Clin. Invest. *128*, 1903–1912. https://doi.org/10.1172/JCI98463.

19. Anfossi, N., André, P., Guia, S., Falk, C.S., Roetynck, S., Stewart, C.A., Breso, V., Frassati, C., Reviron, D., Middleton, D., et al. (2006). Human NK cell education by inhibitory receptors for MHC class I. Immunity *25*, 331–342. https://doi.org/10.1016/j.immuni.2006.06.013.

20. Kim, S., Sunwoo, J.B., Yang, L., Choi, T., Song, Y.J., French, A.R., Vlahiotis, A., Piccirillo, J.F., Cella, M., Colonna, M., et al. (2008). HLA alleles determine differences in human natural killer cell responsiveness and potency. Proc. Natl. Acad. Sci. USA *105*, 3053–3058. https://doi.org/10.1073/pnas.0712229105.

21. Philippon, C., Tao, S., Clement, D., Haroun-Izquierdo, A., Kichula, K.M., Netskar, H., Brandt, L., Oei, V.S., Kanaya, M., Lanuza, P.M., et al. (2023). Allelic variation of KIR and HLA tunes the cytolytic payload and determines functional hierarchy of NK cell repertoires. Blood Adv. *7*, 4492–4504. https://doi.org/10.1182/bloodadvances.2023009827.

22. Martin, M.P., Qi, Y., Gao, X., Yamada, E., Martin, J.N., Pereyra, F., Colombo, S., Brown, E.E., Shupert, W.L., Phair, J., et al. (2007). Innate partnership of HLA-B and KIR3DL1 subtypes against HIV-1. Nat. Genet. *39*, 733–740. https://doi.org/10.1038/ng2035.

23. Boudreau, J.E., Mulrooney, T.J., Le Luduec, J.B., Barker, E., and Hsu, K.C. (2016). KIR3DL1 and HLA-B density and binding calibrate NK education and response to HIV. J. Immunol. *196*, 3398–3410. https://doi.org/10.4049/jimmunol.1502469.

24. Vivian, J.P., Duncan, R.C., Berry, R., O'Connor, G.M., Reid, H.H., Beddoe, T., Gras, S., Saunders, P.M., Olshina, M.A., Widjaja, J.M.L., et al. (2011). Killer cell immunoglobulin-like receptor 3DL1-mediated recognition of human leukocyte antigen B. Nature *479*, 401–405. https://doi.org/10.1038/nature10517.

25. Norman, P.J., Abi-Rached, L., Gendzekhadze, K., Korbel, D., Gleimer, M., Rowley, D., Bruno, D., Carrington, C.V.F., Chandanayingyong, D., Chang, Y.H., et al. (2007). Unusual selection on the KIR3DL1/S1 natural killer cell receptor in Africans. Nat. Genet. *39*, 1092–1099. https://doi.org/10.1038/ng2111.

26. Saunders, P.M., Pymm, P., Pietra, G., Hughes, V.A., Hitchen, C., O'Connor, G.M., Loiacono, F., Widjaja, J., Price, D.A., Falco, M., et al. (2016). Killer cell immunoglobulin-like receptor 3DL1 polymorphism defines distinct hierarchies of HLA class I recognition. J. Exp. Med. *213*, 791–807. https://doi.org/10.1084/jem.20152023.

27. Nemat-Gorgani, N., Edinur, H.A., Hollenbach, J.A., Traherne, J.A., Dunn, P.P.J., Chambers, G.K., Parham, P., and Norman, P.J. (2014). KIR diversity in Maori and Polynesians: populations in which HLA-B is not a significant KIR ligand. Immunogenetics *66*, 597–611. https://doi.org/10.1007/s00251-014-0794-1.

28. Malaspinas, A.S., Westaway, M.C., Muller, C., Sousa, V.C., Lao, O., Alves, I., Bergström, A., Athanasiadis, G., Cheng, J.Y., Crawford, J.E., et al. (2016). A genomic history of Aboriginal Australia. Nature *538*, 207–214. https://doi.org/10.1038/nature18299.

29. Nagle, N., van Oven, M., Wilcox, S., van Holst Pellekaan, S., Tyler-Smith, C., Xue, Y., Ballantyne, K.N., Wilcox, L., Papac, L., Cooke, K., et al. (2017). Aboriginal Australian mitochondrial genome variation - an increased understanding of population antiquity and diversity. Sci. Rep. *7*, 43041. https://doi.org/10.1038/srep43041.

30. Quach, H., Rotival, M., Pothlichet, J., Loh, Y.E., Dannemann, M., Zidane, N., Laval, G., Patin, E., Harmant, C., Lopez, M., et al. (2016). Genetic adaptation and neandertal admixture shaped the immune system of human populations. Cell *167*, 643–656.e17. https://doi.org/10.1016/j.cell.2016.09.024.

31. Hsieh, P., Vollger, M.R., Dang, V., Porubsky, D., Baker, C., Cantsilieris, S., Hoekzema, K., Lewis, A.P., Munson, K.M., Sorensen, M., et al. (2019). Adaptive archaic introgression of copy number variants and the discovery of previously unknown human genes. Science *366*, eaax2083. https://doi.org/10.1126/science.aax2083.

32. Choin, J., Mendoza-Revilla, J., Arauna, L.R., Cuadros-Espinoza, S., Cassar, O., Larena, M., Ko, A.M.S., Harmant, C., Laurent, R., Verdu, P., et al. (2021). Genomic insights into population history and biological adaptation in Oceania. Nature *592*, 583–589. https://doi.org/10.1038/s41586-021-03236-5.

33. Meyer, M., Kircher, M., Gansauge, M.T., Li, H., Racimo, F., Mallick, S., Schraiber, J.G., Jay, F., Prüfer, K., de Filippo, C., et al. (2012). A high-coverage genome sequence from an archaic Denisovan individual. Science *338*, 222–226. https://doi.org/10.1126/science.1224344.

34. Jacobs, G.S., Hudjashov, G., Saag, L., Kusuma, P., Darusallam, C.C., Lawson, D.J., Mondal, M., Pagani, L., Ricaut, F.X., Stoneking, M., et al.

(2019). Multiple deeply divergent denisovan ancestries in Papuans. Cell *177*, 1010–1021.e32. https://doi.org/10.1016/j.cell.2019.02.035.

35. Abi-Rached, L., Jobin, M.J., Kulkarni, S., McWhinnie, A., Dalva, K., Gragert, L., Babrzadeh, F., Gharizadeh, B., Luo, M., Plummer, F.A., et al. (2011). The shaping of modern human immune systems by multiregional admixture with archaic humans. Science *334*, 89–94. https://doi.org/10.1126/science.1209202.
36. Zammit, N.W., Siggs, O.M., Gray, P.E., Horikawa, K., Langley, D.B., Walters, S.N., Daley, S.R., Loetsch, C., Warren, J., Yap, J.Y., et al. (2019). Denisovan, modern human and mouse TNFAIP3 alleles tune A20 phosphorylation and immunity. Nat. Immunol. *20*, 1299–1310. https://doi.org/10.1038/s41590-019-0492-0.
37. Zeberg, H., Jakobsson, M., and Pääbo, S. (2024). The genetic changes that shaped Neandertals, Denisovans, and modern humans. Cell *187*, 1047–1058. https://doi.org/10.1016/j.cell.2023.12.029.
38. Sankararaman, S., Mallick, S., Dannemann, M., Prüfer, K., Kelso, J., Pääbo, S., Patterson, N., and Reich, D. (2014). The genomic landscape of Neanderthal ancestry in present-day humans. Nature *507*, 354–357. https://doi.org/10.1038/nature12961.
39. Vespasiani, D.M., Jacobs, G.S., Cook, L.E., Brucato, N., Leavesley, M., Kinipi, C., Ricaut, F.X., Cox, M.P., and Gallego Romero, I. (2022). Denisovan introgression has shaped the immune system of present-day Papuans. PLoS Genet. *18*, e1010470. https://doi.org/10.1371/journal.pgen.1010470.
40. Prugnolle, F., Manica, A., Charpentier, M., Guégan, J.F., Guernier, V., and Balloux, F. (2005). Pathogen-driven selection and worldwide HLA class I diversity. Curr. Biol. *15*, 1022–1027. https://doi.org/10.1016/j.cub.2005.04.050.
41. Pando, M.J., Gardiner, C.M., Gleimer, M., McQueen, K.L., and Parham, P. (2003). The protein made from a common allele of KIR3DL1 (3DL1*004) is poorly expressed at cell surfaces due to substitution at positions 86 in Ig domain 0 and 182 in Ig domain 1. J. Immunol. *171*, 6640–6649. https://doi.org/10.4049/jimmunol.171.12.6640.
42. Fan, S., Kelly, D.E., Beltrame, M.H., Hansen, M.E.B., Mallick, S., Ranciaro, A., Hirbo, J., Thompson, S., Beggs, W., Nyambo, T., et al. (2019). African evolutionary history inferred from whole genome sequence data of 44 indigenous African populations. Genome Biol. *20*, 82. https://doi.org/10.1186/s13059-019-1679-2.
43. Gao, X., Lester, S., Veale, A., Boettcher, B., Currie, B., McCluskey, J., and Chelvanayagam, G. (2000). HLA class I alleles in Australian Aborigines and their peptide binding profiles. In Major Histocompatibility Complex Evolution, Structure, and Function, M. Kasahara, ed. (Springer) https://doi.org/10.1007/978-4-431-65868-9.
44. Lienert, K., McCluskey, J., Bennett, G., Fowler, C., and Russ, G. (1995). HLA class I variation in Australian Aborigines: characterization of allele B*1521. Tissue Antigens *45*, 12–17. https://doi.org/10.1111/j.1399-0039.1995.tb02409.x.
45. Goodridge, J.P., Jacobs, B., Saetersmoen, M.L., Clement, D., Hammer, Q., Clancy, T., Skarpen, E., Brech, A., Landskron, J., Grimm, C., et al. (2019). Remodeling of secretory lysosomes during education tunes functional potential in NK cells. Nat. Commun. *10*, 514. https://doi.org/10.1038/s41467-019-08384-x.
46. Yawata, M., Yawata, N., Draghi, M., Little, A.M., Partheniou, F., and Parham, P. (2006). Roles for HLA and KIR polymorphisms in natural killer cell repertoire selection and modulation of effector function. J. Exp. Med. *203*, 633–645. https://doi.org/10.1084/jem.20051884.
47. Parham, P., Norman, P.J., Abi-Rached, L., and Guethlein, L.A. (2011). Variable NK cell receptors exemplified by human KIR3DL1/S1. J. Immunol. *187*, 11–19. https://doi.org/10.4049/jimmunol.0902332.
48. Saunders, P.M., MacLachlan, B.J., Widjaja, J., Wong, S.C., Oates, C.V.L., Rossjohn, J., Vivian, J.P., and Brooks, A.G. (2021). The role of the HLA class I alpha2 helix in determining ligand hierarchy for the killer cell Ig-like receptor 3DL1. J. Immunol. *206*, 849–860. https://doi.org/10.4049/jimmunol.2001109.
49. Quinto-Cortés, C.D., Jonas, C.B., Vieyra-Sánchez, S., Oppenheimer, S., González-Buenfil, R., Auckland, K., Robson, K., Parks, T., Moreno-Mayar, J.V., and Blanco-Portillo, J. (2024). The Genomic Landscape of Oceania. Preprint at arXiv. https://doi.org/10.48550/arXiv.2405.09216.
50. Bergström, A., Oppenheimer, S.J., Mentzer, A.J., Auckland, K., Robson, K., Attenborough, R., Alpers, M.P., Koki, G., Pomat, W., Siba, P., et al. (2017). A Neolithic expansion, but strong genetic structure, in the independent history of New Guinea. Science *357*, 1160–1163. https://doi.org/10.1126/science.aan3842.
51. Robinson, J., Halliwell, J.A., Hayhurst, J.D., Flicek, P., Parham, P., and Marsh, S.G. (2015). The IPD and IMGT/HLA database: allele variant databases. Nucleic Acids Res. *43*, D423–D431. https://doi.org/10.1093/nar/gku1161.
52. Browning, S.R., Browning, B.L., Zhou, Y., Tucci, S., and Akey, J.M. (2018). Analysis of human sequence data reveals two pulses of archaic denisovan admixture. Cell *173*, 53–61.e9. https://doi.org/10.1016/j.cell.2018.02.031.
53. Reich, D., Green, R.E., Kircher, M., Krause, J., Patterson, N., Durand, E.Y., Viola, B., Briggs, A.W., Stenzel, U., Johnson, P.L.F., et al. (2010). Genetic history of an archaic hominin group from Denisova Cave in Siberia. Nature *468*, 1053–1060. https://doi.org/10.1038/nature09710.
54. Patterson, N., Moorjani, P., Luo, Y., Mallick, S., Rohland, N., Zhan, Y., Genschoreck, T., Webster, T., and Reich, D. (2012). Ancient admixture in human history. Genetics *192*, 1065–1093. https://doi.org/10.1534/genetics.112.145037.
55. Huerta-Sánchez, E., Jin, X., Asan, X., Bianba, Z., Peter, B.M., Vinckenbosch, N., Liang, Y., Yi, X., He, M., Somel, M., et al. (2014). Altitude adaptation in Tibetans caused by introgression of Denisovan-like DNA. Nature *512*, 194–197. https://doi.org/10.1038/nature13408.
56. Solberg, O.D., Mack, S.J., Lancaster, A.K., Single, R.M., Tsai, Y., Sanchez-Mazas, A., and Thomson, G. (2008). Balancing selection and heterogeneity across the classical human leukocyte antigen loci: a meta-analytic review of 497 population studies. Hum. Immunol. *69*, 443–464. https://doi.org/10.1016/j.humimm.2008.05.001.
57. Viard, M., O'HUigin, C., Yuki, Y., Bashirova, A.A., Collins, D.R., Urbach, J.M., Wolinsky, S., Buchbinder, S., Kirk, G.D., Goedert, J.J., et al. (2024). Impact of HLA class I functional divergence on HIV control. Science *383*, 319–325. https://doi.org/10.1126/science.adk0777.
58. Pierini, F., and Lenz, T.L. (2018). Divergent allele advantage at human MHC genes: signatures of past and ongoing selection. Mol. Biol. Evol. *35*, 2145–2158. https://doi.org/10.1093/molbev/msy116.
59. Bugawan, T.L., Mack, S.J., Stoneking, M., Saha, M., Beck, H.P., and Erlich, H.A. (1999). HLA class I allele distributions in six Pacific/Asian populations: evidence of selection at the HLA-A locus. Tissue Antigens *53*, 311–319. https://doi.org/10.1034/j.1399-0039.1999.530401.x.
60. Hensen, L., Illing, P.T., Bridie Clemens, E., Nguyen, T.H.O., Koutsakos, M., van de Sandt, C.E., Mifsud, N.A., Nguyen, A.T., Szeto, C., Chua, B.Y., et al. (2021). CD8(+) T cell landscape in Indigenous and non-indigenous people restricted by influenza mortality-associated HLA-A*24:02 allomorph. Nat. Commun. *12*, 2931. https://doi.org/10.1038/s41467-021-23212-x.
61. Saunders, P.M., MacLachlan, B.J., Pymm, P., Illing, P.T., Deng, Y., Wong, S.C., Oates, C.V.L., Purcell, A.W., Rossjohn, J., Vivian, J.P., et al. (2020). The molecular basis of how buried human leukocyte antigen polymorphism modulates natural killer cell function. Proc. Natl. Acad. Sci. USA *117*, 11636–11647. https://doi.org/10.1073/pnas.1920570117.
62. Sharma, D., Bastard, K., Guethlein, L.A., Norman, P.J., Yawata, N., Yawata, M., Pando, M., Thananchai, H., Dong, T., Rowland-Jones, S., et al. (2009). Dimorphic motifs in D0 and D1+D2 domains of killer cell Ig-like receptor 3DL1 combine to form receptors with high, moderate, and no avidity for the complex of a peptide derived from HIV and HLA-a*2402. J. Immunol. *183*, 4569–4582. https://doi.org/10.4049/jimmunol.0901734.

63. Khakoo, S.I., Thio, C.L., Martin, M.P., Brooks, C.R., Gao, X., Astemborski, J., Cheng, J., Goedert, J.J., Vlahov, D., Hilgartner, M., et al. (2004). HLA and NK cell inhibitory receptor genes in resolving hepatitis C virus infection. Science *305*, 872–874. https://doi.org/10.1126/science.1097670.

64. Tano-Menka, R., Singh, N.K., Muzhingi, I., Li, X., Mandanas, M.V., Kaseke, C., Crain, C.R., Zhang, A., Ogunshola, F.J., Vecchiarello, L., et al. (2024). Polymorphic residues in HLA-B that mediate HIV control distinctly modulate peptide interactions with both TCR and KIR molecules. Structure *32*, 1121–1136.e5. https://doi.org/10.1016/j.str.2024.04.015.

65. Li, J., Zaslavsky, M., Su, Y., Guo, J., Sikora, M.J., van Unen, V., Christophersen, A., Chiou, S.H., Chen, L., Li, J., et al. (2022). KIR(+)CD8(+) T cells suppress pathogenic T cells and are active in autoimmune diseases and COVID-19. Science *376*, eabi9591. https://doi.org/10.1126/science.abi9591.

66. Ali, A., Gyurova, I.E., and Waggoner, S.N. (2019). Mutually assured destruction: the cold war between viruses and natural killer cells. Curr. Opin. Virol. *34*, 130–139. https://doi.org/10.1016/j.coviro.2019.02.005.

67. Scharenberg, M., Vangeti, S., Kekäläinen, E., Bergman, P., Al-Ameri, M., Johansson, N., Sondén, K., Falck-Jones, S., Färnert, A., Ljunggren, H.G., et al. (2019). Influenza A virus infection induces hyperresponsiveness in human lung tissue-resident and peripheral blood NK cells. Front. Immunol. *10*, 1116. https://doi.org/10.3389/fimmu.2019.01116.

68. Palmer, W.H., Leaton, L.A., Campos Codo, A., Crute, B., Roest, J., Zhu, S., Petersen, J., Tobin, R.P., Hume, P.S., Stone, M., et al. (2023). Polymorphic KIR3DL3 expression modulates tissue-resident and innate-like T cells. Sci. Immunol. *8*, eade5343. https://doi.org/10.1126/sciimmunol.ade5343.

69. Digitale, J.C., Callaway, P.C., Martin, M., Nelson, G., Viard, M., Rek, J., Arinaitwe, E., Dorsey, G., Kamya, M., Carrington, M., et al. (2020). Inhibitory KIR ligands are associated with higher P. falciparum parasite prevalence. J. Infect. Dis. https://doi.org/10.1093/infdis/jiaa698.

70. Anderson, K.M., Augusto, D.G., Dandekar, R., Shams, H., Zhao, C., Yusufali, T., Montero-Martín, G., Marin, W.M., Nemat-Gorgani, N., Creary, L.E., et al. (2020). Killer cell immunoglobulin-like receptor variants are associated with protection from symptoms associated with more severe course in Parkinson disease. J. Immunol. *205*, 1323–1330. https://doi.org/10.4049/jimmunol.2000144.

71. Ahn, R.S., Moslehi, H., Martin, M.P., Abad-Santos, M., Bowcock, A.M., Carrington, M., and Liao, W. (2016). Inhibitory KIR3DL1 alleles are associated with psoriasis. Br. J. Dermatol. *174*, 449–451. https://doi.org/10.1111/bjd.14081.

72. Boudreau, J.E., Giglio, F., Gooley, T.A., Stevenson, P.A., Le Luduec, J.B., Shaffer, B.C., Rajalingam, R., Hou, L., Hurley, C.K., Noreen, H., et al. (2017). KIR3DL1/HLA-B subtypes govern acute myelogenous leukemia relapse after hematopoietic cell transplantation. J. Clin. Oncol. *35*, 2268–2278. https://doi.org/10.1200/JCO.2016.70.7059.

73. Forlenza, C.J., Boudreau, J.E., Zheng, J., Le Luduec, J.B., Chamberlain, E., Heller, G., Cheung, N.K.V., and Hsu, K.C. (2016). KIR3DL1 allelic polymorphism and HLA-B epitopes modulate response to anti-GD2 monoclonal antibody in patients with neuroblastoma. J. Clin. Oncol. *34*, 2443–2451. https://doi.org/10.1200/JCO.2015.64.9558.

74. Trefny, M.P., Rothschild, S.I., Uhlenbrock, F., Rieder, D., Kasenda, B., Stanczak, M.A., Berner, F., Kashyap, A.S., Kaiser, M., Herzig, P., et al. (2019). A variant of a killer cell immunoglobulin-like receptor is associated with resistance to PD-1 blockade in lung cancer. Clin. Cancer Res. *25*, 3026–3034. https://doi.org/10.1158/1078-0432.CCR-18-3041.

75. Iuliano, A.D., Roguski, K.M., Chang, H.H., Muscatello, D.J., Palekar, R., Tempia, S., Cohen, C., Gran, J.M., Schanzer, D., Cowling, B.J., et al. (2018). Estimates of global seasonal influenza-associated respiratory mortality: a modelling study. Lancet *391*, 1285–1300. https://doi.org/10.1016/S0140-6736(17)33293-2.

76. Schultz-Cherry, S. (2015). Role of NK cells in influenza infection. Curr. Top. Microbiol. Immunol. *386*, 109–120. https://doi.org/10.1007/82_2014_403.

77. Frank, K., and Paust, S. (2020). Dynamic natural killer cell and T cell responses to influenza infection. Front. Cell. Infect. Microbiol. *10*, 425. https://doi.org/10.3389/fcimb.2020.00425.

78. Mandelboim, O., Lieberman, N., Lev, M., Paul, L., Arnon, T.I., Bushkin, Y., Davis, D.M., Strominger, J.L., Yewdell, J.W., and Porgador, A. (2001). Recognition of haemagglutinins on virus-infected cells by NKp46 activates lysis by human NK cells. Nature *409*, 1055–1060. https://doi.org/10.1038/35059110.

79. Loh, L., Wang, Z., Sant, S., Koutsakos, M., Jegaskanda, S., Corbett, A.J., Liu, L., Fairlie, D.P., Crowe, J., Rossjohn, J., et al. (2016). Human mucosal-associated invariant T cells contribute to antiviral influenza immunity via IL-18-dependent activation. Proc. Natl. Acad. Sci. USA *113*, 10133–10138. https://doi.org/10.1073/pnas.1610750113.

80. Guo, H., Kumar, P., and Malarkannan, S. (2010). Evasion of natural killer cells by influenza virus. J. Leukoc. Biol. *89*, 189–194. https://doi.org/10.1189/jlb.0610319.

81. Dong, L., Mori, I., Hossain, M.J., and Kimura, Y. (2000). The senescence-accelerated mouse shows aging-related defects in cellular but not humoral immunity against influenza virus infection. J. Infect. Dis. *182*, 391–396. https://doi.org/10.1086/315727.

82. Achdout, H., Manaster, I., and Mandelboim, O. (2008). Influenza virus infection augments NK cell inhibition through reorganization of major histocompatibility complex class I proteins. J. Virol. *82*, 8030–8037. https://doi.org/10.1128/JVI.00870-08.

83. Hilton, H.G., Vago, L., Older Aguilar, A.M., Moesta, A.K., Graef, T., Abi-Rached, L., Norman, P.J., Guethlein, L.A., Fleischhauer, K., and Parham, P. (2012). Mutation at positively selected positions in the binding site for HLA-C shows that KIR2DL1 is a more refined but less adaptable NK cell receptor than KIR2DL3. J. Immunol. *189*, 1418–1430. https://doi.org/10.4049/jimmunol.1100431.

84. Ahlenstiel, G., Martin, M.P., Gao, X., Carrington, M., and Rehermann, B. (2008). Distinct KIR/HLA compound genotypes affect the kinetics of human antiviral natural killer cell responses. J. Clin. Invest. *118*, 1017–1026. https://doi.org/10.1172/JCI32400.

85. Single, R.M., Martin, M.P., Gao, X., Meyer, D., Yeager, M., Kidd, J.R., Kidd, K.K., and Carrington, M. (2007). Global diversity and evidence for coevolution of KIR and HLA. Nat. Genet. *39*, 1114–1119. https://doi.org/10.1038/ng2077.

86. Fu, W., and Akey, J.M. (2013). Selection and adaptation in the human genome. Annu. Rev. Genomics Hum. Genet. *14*, 467–489. https://doi.org/10.1146/annurev-genom-091212-153509.

87. Parham, P., Barnstable, C.J., and Bodmer, W.F. (1979). Use of a monoclonal antibody (W6/32) in structural studies of HLA-A,B,C, antigens. J. Immunol. *123*, 342–349.

88. Zernich, D., Purcell, A.W., Macdonald, W.A., Kjer-Nielsen, L., Ely, L.K., Laham, N., Crockford, T., Mifsud, N.A., Bharadwaj, M., Chang, L., et al. (2004). Natural HLA class I polymorphism controls the pathway of antigen presentation and susceptibility to viral evasion. J. Exp. Med. *200*, 13–24. https://doi.org/10.1084/jem.20031680.

89. Ellis, S.A., Taylor, C., and McMichael, A. (1982). Recognition of HLA-B27 and related antigen by a monoclonal antibody. Hum. Immunol. *5*, 49–59. https://doi.org/10.1016/0198-8859(82)90030-1.

90. Kostenko, L., Kjer-Nielsen, L., Nicholson, I., Hudson, F., Lucas, A., Foley, B., Chen, K., Lynch, K., Nguyen, J., Wu, A.H., et al. (2011). Rapid screening for the detection of HLA-B57 and HLA-B58 in prevention of drug hypersensitivity. Tissue Antigens *78*, 11–20. https://doi.org/10.1111/j.1399-0039.2011.01649.x.

91. La Gruta, N.L., Liu, H., Dilioglou, S., Rhodes, M., Wiest, D.L., and Vignali, D.A.A. (2004). Architectural changes in the TCR:CD3 complex induced

by MHC:peptide ligation. J. Immunol. *172*, 3662–3669. https://doi.org/10.4049/jimmunol.172.6.3662.

92. Robinson, J., Barker, D.J., and Marsh, S.G.E. (2024). 25 years of the IPD-IMGT/HLA Database. HLA *103*, e15549. https://doi.org/10.1111/tan.15549.
93. Mack, S.J., and Erlich, H.A. (2007). Anthropology/human genetic diversity joint report. In Immunobiology of the MHC Proceedings of the 13th International Histocompatibility Workshop and Conference, J.A. Hansen, ed. (IHWG Press), pp. 557–766.
94. Byrska-Bishop, M., Evani, U.S., Zhao, X., Basile, A.O., Abel, H.J., Regier, A.A., Corvelo, A., Clarke, W.E., Musunuri, R., Nagulapalli, K., et al. (2022). High-coverage whole-genome sequencing of the expanded 1000 Genomes Project cohort including 602 trios. Cell *185*, 3426–3440.e19. https://doi.org/10.1016/j.cell.2022.08.004.
95. Mallick, S., Li, H., Lipson, M., Mathieson, I., Gymrek, M., Racimo, F., Zhao, M., Chennagiri, N., Nordenfelt, S., Tandon, A., et al. (2016). The Simons Genome Diversity Project: 300 genomes from 142 diverse populations. Nature *538*, 201–206. https://doi.org/10.1038/nature18964.
96. Norman, P.J., Hollenbach, J.A., Nemat-Gorgani, N., Guethlein, L.A., Hilton, H.G., Pando, M.J., Koram, K.A., Riley, E.M., Abi-Rached, L., and Parham, P. (2013). Co-evolution of human leukocyte antigen (HLA) class I ligands with killer-cell immunoglobulin-like receptors (KIR) in a genetically diverse population of sub-Saharan Africans. PLoS Genet. *9*, e1003938. https://doi.org/10.1371/journal.pgen.1003938.
97. Nemat-Gorgani, N., Hilton, H.G., Henn, B.M., Lin, M., Gignoux, C.R., Myrick, J.W., Werely, C.J., Granka, J.M., Moller, M., Hoal, E.G., et al. (2018). Different selected mechanisms attenuated the inhibitory interaction of KIR2DL1 with C2(+) HLA-C in two indigenous human populations in Southern Africa. J. Immunol. *200*, 2640–2655. https://doi.org/10.4049/jimmunol.1701780.
98. Gendzekhadze, K., Norman, P.J., Abi-Rached, L., Graef, T., Moesta, A.K., Layrisse, Z., and Parham, P. (2009). Co-evolution of KIR2DL3 with HLA-C in a human population retaining minimal essential diversity of KIR and HLA class I ligands. Proc. Natl. Acad. Sci. USA *106*, 18692–18697. https://doi.org/10.1073/pnas.0906051106.
99. Deng, Z., Zhen, J., Harrison, G.F., Zhang, G., Chen, R., Sun, G., Yu, Q., Nemat-Gorgani, N., Guethlein, L.A., He, L., et al. (2021). Adaptive admixture of HLA Class I allotypes enhanced genetically determined strength of natural killer cells in East Asians. Mol. Biol. Evol. *38*, 2582–2596. https://doi.org/10.1093/molbev/msab053.
100. Amorim, L.M., Augusto, D.G., Nemat-Gorgani, N., Montero-Martin, G., Marin, W.M., Shams, H., Dandekar, R., Caillier, S., Parham, P., Fernández-Viña, M.A., et al. (2021). High-resolution characterization of KIR genes in a large North American cohort reveals novel details of structural and sequence diversity. Front. Immunol. *12*, 674778. https://doi.org/10.3389/fimmu.2021.674778.
101. Tao, S., Kichula, K.M., Harrison, G.F., Farias, T.D.J., Palmer, W.H., Leaton, L.A., Hajar, C.G.N., Zefarina, Z., Edinur, H.A., Zhu, F., et al. (2021). The combinatorial diversity of KIR and HLA class I allotypes in Peninsular Malaysia. Immunology *162*, 389–404. https://doi.org/10.1111/imm.13289.
102. Norman, P.J., Hollenbach, J.A., Nemat-Gorgani, N., Marin, W.M., Norberg, S.J., Ashouri, E., Jayaraman, J., Wroblewski, E.E., Trowsdale, J., Rajalingam, R., et al. (2016). Defining KIR and HLA Class I genotypes at highest resolution via high-throughput sequencing. Am. J. Hum. Genet. *99*, 375–391. https://doi.org/10.1016/j.ajhg.2016.06.023.
103. de Brito Vargas, L.B., Beltrame, M.H., Ho, B., Marin, W.M., Dandekar, R., Montero-Martín, G., Fernández-Viña, M.A., Hurtado, A.M., Hill, K.R., Tsuneto, L.T., et al. (2022). Remarkably low KIR and HLA diversity in Amerindians reveals signatures of strong purifying selection shaping the centromeric KIR region. Mol. Biol. Evol. *39*, msab298. https://doi.org/10.1093/molbev/msab298.
104. Nemat-Gorgani, N., Guethlein, L.A., Henn, B.M., Norberg, S.J., Chiaroni, J., Sikora, M., Quintana-Murci, L., Mountain, J.L., Norman, P.J., and Parham, P. (2019). Diversity of KIR, HLA Class I, and their interactions in seven populations of sub-Saharan Africans. J. Immunol. *202*, 2636–2647. https://doi.org/10.4049/jimmunol.1801586.
105. Shimizu, Y., and DeMars, R. (1989). Production of human cells expressing individual transferred HLA-A,-B,-C genes using an HLA-A,-B,-C null human cell line. J. Immunol. *142*, 3320–3328.
106. Saunders, P.M., Vivian, J.P., Baschuk, N., Beddoe, T., Widjaja, J., O'Connor, G.M., Hitchen, C., Pymm, P., Andrews, D.M., Gras, S., et al. (2015). The interaction of KIR3DL1*001 with HLA class I molecules is dependent upon molecular microarchitecture within the Bw4 epitope. J. Immunol. *194*, 781–789. https://doi.org/10.4049/jimmunol.1402542.
107. Macdonald, W.A., Chen, Z., Gras, S., Archbold, J.K., Tynan, F.E., Clements, C.S., Bharadwaj, M., Kjer-Nielsen, L., Saunders, P.M., Wilce, M.C.J., et al. (2009). T cell allorecognition via molecular mimicry. Immunity *31*, 897–908. https://doi.org/10.1016/j.immuni.2009.09.025.
108. O'Connor, G.M., Guinan, K.J., Cunningham, R.T., Middleton, D., Parham, P., and Gardiner, C.M. (2007). Functional polymorphism of the KIR3DL1/S1 receptor on human NK cells. J. Immunol. *178*, 235–241.
109. Williams, A.P., Peh, C.A., Purcell, A.W., McCluskey, J., and Elliott, T. (2002). Optimization of the MHC class I peptide cargo is dependent on tapasin. Immunity *16*, 509–520. https://doi.org/10.1016/S1074-7613(02)00304-7.
110. Studier, F.W., and Moffatt, B.A. (1986). Use of bacteriophage T7 RNA polymerase to direct selective high-level expression of cloned genes. J. Mol. Biol. *189*, 113–130. https://doi.org/10.1016/0022-2836(86)90385-2.
111. Marin, W.M., Dandekar, R., Augusto, D.G., Yusufali, T., Heyn, B., Hofmann, J., Lange, V., Sauter, J., Norman, P.J., and Hollenbach, J.A. (2021). High-throughput interpretation of killer-cell immunoglobulin-like receptor short-read sequencing data with PING. PLoS Comput. Biol. *17*, e1008904. https://doi.org/10.1371/journal.pcbi.1008904.
112. Harrison, G.F., Leaton, L.A., Harrison, E.A., Kichula, K.M., Viken, M.K., Shortt, J., Gignoux, C.R., Lie, B.A., Vukcevic, D., Leslie, S., et al. (2022). Allele imputation for the killer cell immunoglobulin-like receptor KIR3DL1/S1. PLoS Comput. Biol. *18*, e1009059. https://doi.org/10.1371/journal.pcbi.1009059.
113. Falush, D., Stephens, M., and Pritchard, J.K. (2007). Inference of population structure using multilocus genotype data: dominant markers and null alleles. Mol. Ecol. Notes *7*, 574–578.
114. Tamura, K., Stecher, G., Peterson, D., Filipski, A., and Kumar, S. (2013). MEGA6: molecular evolutionary genetics analysis version 6.0. Mol. Biol. Evol. *30*, 2725–2729. https://doi.org/10.1093/molbev/mst197.
115. Chang, C.C., Chow, C.C., Tellier, L.C.A.M., Vattikuti, S., Purcell, S.M., and Lee, J.J. (2015). Second-generation PLINK: rising to the challenge of larger and richer datasets. GigaScience *4*, 7. https://doi.org/10.1186/s13742-015-0047-8.
116. Manichaikul, A., Mychaleckyj, J.C., Rich, S.S., Daly, K., Sale, M., and Chen, W.-M. (2010). Robust relationship inference in genome-wide association studies. Bioinformatics *26*, 2867–2873. https://doi.org/10.1093/bioinformatics/btq559.
117. Zheng, X., Shen, J., Cox, C., Wakefield, J.C., Ehm, M.G., Nelson, M.R., and Weir, B.S. (2014). HIBAG—HLA genotype imputation with attribute bagging. Pharmacogenomics J. *14*, 192–200. https://doi.org/10.1038/tpj.2013.18.
118. Taliun, D., Harris, D.N., Kessler, M.D., Carlson, J., Szpiech, Z.A., Torres, R., Taliun, S.A.G., Corvelo, A., Gogarten, S.M., Kang, H.M., et al. (2021). Sequencing of 53,831 diverse genomes from the NHLBI TOPMed Program. Nature *590*, 290–299. https://doi.org/10.1038/s41586-021-03205-y.
119. Wessel, P., and Smith, W.H.F. (1998). New, improved version of generic mapping tools released. Eos Trans. Am. Geophys. Union *79*, 579. https://doi.org/10.1029/98EO00426.

120. Alexander, D.H., Novembre, J., and Lange, K. (2009). Fast model-based estimation of ancestry in unrelated individuals. Genome Res. *19*, 1655–1664. https://doi.org/10.1101/gr.094052.109.

121. Behr, A.A., Liu, K.Z., Liu-Fang, G., Nakka, P., and Ramachandran, S. (2016). pong: fast analysis and visualization of latent clusters in population genetic data. Bioinformatics *32*, 2817–2823. https://doi.org/10.1093/bioinformatics/btw327.

122. Maples, B.K., Gravel, S., Kenny, E.E., and Bustamante, C.D. (2013). RFMix: a discriminative modeling approach for rapid and robust local-ancestry inference. Am. J. Hum. Genet. *93*, 278–288. https://doi.org/10.1016/j.ajhg.2013.06.020.

123. Delaneau, O., Zagury, J.-F., Robinson, M.R., Marchini, J.L., and Dermitzakis, E.T. (2019). Accurate, scalable and integrative haplotype estimation. Nat. Commun. *10*, 5436. https://doi.org/10.1038/s41467-019-13225-y.

124. Danecek, P., Bonfield, J.K., Liddle, J., Marshall, J., Ohan, V., Pollard, M.O., Whitwham, A., Keane, T., McCarthy, S.A., Davies, R.M., et al. (2021). Twelve years of SAMtools and BCFtools. GigaScience *10*, giab008. https://doi.org/10.1093/gigascience/giab008.

125. Tamura, K., Stecher, G., and Kumar, S. (2021). MEGA11: Molecular Evolutionary Genetics Analysis, version 11. Mol. Biol. Evol. *38*, 3022–3027. https://doi.org/10.1093/molbev/msab120.

126. Yang, Z. (2007). PAML 4: Phylogenetic analysis by maximum likelihood. Mol. Biol. Evol. *24*, 1586–1591. https://doi.org/10.1093/molbev/msm088.

127. Excoffier, L., Laval, G., and Schneider, S. (2007). Arlequin (version 3.0): an integrated software package for population genetics data analysis. Evol. Bioinform. Online *1*, 47–50.

128. Danecek, P., Auton, A., Abecasis, G., Albers, C.A., Banks, E., DePristo, M.A., Handsaker, R.E., Lunter, G., Marth, G.T., Sherry, S.T., et al. (2011). The variant call format and VCFtools. Bioinformatics *27*, 2156–2158. https://doi.org/10.1093/bioinformatics/btr330.

129. Szpiech, Z.A., and Hernandez, R.D. (2014). selscan: an Efficient Multithreaded Program to Perform EHH-Based Scans for Positive Selection. Mol. Biol. Evol. *31*, 2824–2827. https://doi.org/10.1093/molbev/msu211.

130. Kabsch, W. (2010). XDS. Acta Crystallogr. D Biol. Crystallogr. *66*, 125–132. https://doi.org/10.1107/S0907444909047337.

131. Collaborative Computational Project, Number 4 (1994). The CCP4 suite: programs for protein crystallography. Acta Crystallogr. D Biol. Crystallogr. *50*, 760–763. https://doi.org/10.1107/S0907444994003112.

132. Adams, P.D., Afonine, P.V., Bunkóczi, G., Chen, V.B., Davis, I.W., Echols, N., Headd, J.J., Hung, L.W., Kapral, G.J., Grosse-Kunstleve, R.W., et al. (2010). Phenix: a comprehensive Python-based system for macromolecular structure solution. Acta Crystallogr. D Biol. Crystallogr. *66*, 213–221. https://doi.org/10.1107/S0907444909052925.

133. Emsley, P., and Cowtan, K. (2004). Coot: model-building tools for molecular graphics. Acta Crystallogr. D Biol. Crystallogr. *60*, 2126–2132. https://doi.org/10.1107/S0907444904019158.

134. Boudreau, J.E., Le Luduec, J.B., and Hsu, K.C. (2014). Development of a novel multiplex PCR assay to detect functional subtypes of KIR3DL1 alleles. PLoS One *9*, e99543. https://doi.org/10.1371/journal.pone.0099543.

135. Gonzalez-Galarza, F.F., McCabe, A., Melo dos Santos, E.J., Jones, A.R., and Middleton, D. (2021). A snapshot of human leukocyte antigen (HLA) diversity using data from the Allele Frequency Net Database. Hum. Immunol. *82*, 496–504. https://doi.org/10.1016/j.humimm.2020.10.004.

136. Auton, A., Abecasis, G.R., Altshuler, D.M., Durbin, R.M., Abecasis, G.R., Bentley, D.R., Chakravarti, A., Clark, A.G., Donnelly, P., Eichler, E.E., et al. (2015). A global reference for human genetic variation. Nature *526*, 68–74. https://doi.org/10.1038/nature15393.

137. Rannala, B., and Yang, Z. (2007). Inferring speciation times under an episodic molecular clock. Syst. Biol. *56*, 453–466. https://doi.org/10.1080/10635150701420643.

138. Benton, M.J., and Donoghue, P.C.J. (2007). Paleontological evidence to date the tree of life. Mol. Biol. Evol. *24*, 26–53. https://doi.org/10.1093/molbev/msl150.

139. Wilson, M.J., Torkar, M., Haude, A., Milne, S., Jones, T., Sheer, D., Beck, S., and Trowsdale, J. (2000). Plasticity in the organization and sequences of human KIR/ILT gene families. Proc. Natl. Acad. Sci. USA *97*, 4778–4783. https://doi.org/10.1073/pnas.080588597.

140. Auton, A., and McVean, G. (2007). Recombination rate estimation in the presence of hotspots. Genome Res. *17*, 1219–1227. https://doi.org/10.1101/gr.6386707.

141. Kong, A., Thorleifsson, G., Gudbjartsson, D.F., Masson, G., Sigurdsson, A., Jonasdottir, A., Walters, G.B., Jonasdottir, A., Gylfason, A., Kristinsson, K.T., et al. (2010). Fine-scale recombination rate differences between sexes, populations and individuals. Nature *467*, 1099–1103. https://doi.org/10.1038/nature09525.

142. Quinto-Cortés, C.D., Woerner, A.E., Watkins, J.C., and Hammer, M.F. (2018). Modeling SNP array ascertainment with Approximate Bayesian Computation for demographic inference. Sci. Rep. *8*, 10209. https://doi.org/10.1038/s41598-018-28539-y.

143. Lachance, J., and Tishkoff, S.A. (2013). SNP ascertainment bias in population genetic analyses: why it is important, and how to correct it. BioEssays *35*, 780–786. https://doi.org/10.1002/bies.201300014.

144. Albrechtsen, A., Nielsen, F.C., and Nielsen, R. (2010). Ascertainment biases in SNP chips affect measures of population divergence. Mol. Biol. Evol. *27*, 2534–2547. https://doi.org/10.1093/molbev/msq148.

145. Voight, B.F., Kudaravalli, S., Wen, X., and Pritchard, J.K. (2006). A map of recent positive selection in the human genome. PLoS Biol. *4*, e72. https://doi.org/10.1371/journal.pbio.0040072.

146. Alter, G., Malenfant, J.M., and Altfeld, M. (2004). CD107a as a functional marker for the identification of natural killer cell activity. J. Immunol. Methods *294*, 15–22. https://doi.org/10.1016/j.jim.2004.08.008.

147. Holst, J., Szymczak-Workman, A.L., Vignali, K.M., Burton, A.R., Workman, C.J., and Vignali, D.A.A. (2006). Generation of T-cell receptor retrogenic mice. Nat. Protoc. *1*, 406–417. https://doi.org/10.1038/nprot.2006.61.

148. Clements, C.S., Kjer-Nielsen, L., MacDonald, W.A., Brooks, A.G., Purcell, A.W., McCluskey, J., and Rossjohn, J. (2002). The production, purification and crystallization of a soluble heterodimeric form of a highly selected T-cell receptor in its unliganded and liganded state. Acta Crystallogr. D Biol. Crystallogr. *58*, 2131–2134. https://doi.org/10.1107/S0907444902015482.

149. R Development Core Team (2021). A Language and Environment for Statistical Computing (R Foundation for Statistical Computing).

STAR★METHODS

KEY RESOURCES TABLE

REAGENT or RESOURCE	SOURCE	IDENTIFIER
Antibodies		
pan-HLA Class 1 W6/32	Parham et al.[87]	N/A
Bw4 RM7.9.63	Zernich et al.[88]	N/A
HLA-B*27 ME1	Ellis et al.[89]	N/A
HLA-B*57/58 (B17 Serotype) 3E12	Kostenko et al.[90]	N/A
Goat anti-mouse IgG-FITC	Millipore	Cat# AP127F, RRID:AB_92468
Mouse IgM-PE	Jackson ImmunoResearch	Cat#115-116-075, RRID: AB_2338628
HLA-C/E DT-9 PE	BD Biosciences	Cat#566372; RRID: AB_2739715
CD107a H4A3 PE-Cy5	BD Biosciences	Cat# 555802, RRID:AB_396136
KIR3DL1(NKB1) DX9 FITC	BD Biosciences	Cat# 340483, RRID:AB_2130832
KIR2DL2/L3/S2 GL183 PE-Cy5.5	Beckman Coulter	Cat# A66900, RRID:AB_2857331
KIR2DL1/S1 EB6B PE-Cy7	Beckman Coulter	Cat# A66899, RRID:AB_3136596
LILRB1 HP-F1 APC	ThermoFisher	Cat# 17-5129-42, RRID:AB_1311214
NKG2A Z199 PE	Beckman Coulter	Cat# IM3291U, RRID:AB_10643228
CD56 NCAM16.2 BV785	BD Biosciences	BD Biosciences Cat# 564058, RRID:AB_2738569
CD3 UCHT1 Pacific Blue	BioLegend	BioLegend Cat# 980004, RRID:AB_3136596
CD3 SK7 APC-Cy7	BD Biosciences	Cat# 341110, RRID:AB_2868766
IFN-γ B27 AF700	BD Biosciences	Cat# 557995, RRID:AB_396977
Purified KIR3DL1 (NKB1) DX9	BD Biosciences	Cat#555964, RRID:AB_396258
CD158e/k 5.133 PE	Miltenyi Biotec	Cat# 130-095-205, RRID:AB_10839570
CD69 FN50 PE	BD Biosciences	Cat#555531, RRID:AB_395916
Bacterial and virus strains		
E.coli BL21 (DE3)	Agilent	Cat#200131
pMIGII	La Gruta et al.[91]	N/A
pPAM-E	La Gruta et al.[91]	N/A
pVSVG	La Gruta et al.[91]	N/A
Biological samples		
Human peripheral blood samples from healthy Australian First Nations Looking Into inFluenza T-cell immunity (LIFT) cohort	Royal Darwin Hospital Outpatient Clinic; Clemens et al.[7] (#HREC-2012-1928; #1441452.1; #0931311.5)	N/A
Human peripheral blood samples from healthy individuals	Australian Red Cross LifeBlood (West Melbourne, Australia)	N/A
Human DNA from Papuan Donors	Institute for Medical Research, Papua New Guinea, Oxford Tropical Research Bergström et al.[50]	N/A
Chemicals, peptides, and recombinant proteins		
Recombinant human IL2	Miltenyi Biotec	Cat#130-097-743
Phytohemagglutinin	ThermoFisher	Cat#10576015
EcoRI-HF	New England Biolabs	Cat#R3101S
BamHI-HF	New England Biolabs	Cat#R3136S
Geneticin (G418 sulfate)	ThermoFisher	Cat#11811098
Golgi Stop	BD Biosciences	Cat#554724
Fixable Live/Dead Aqua Blue viability dye	Life Technologies	Cat#L34957

(*Continued on next page*)

Continued

REAGENT or RESOURCE	SOURCE	IDENTIFIER
Fixable Live/Dead eFluor780 viability dye	Life Technologies	Cat#65-0865-14
Urea	Sigma Aldrich	Cat#57.13.6
Trisma Base	Sigma Aldrich	Cat#77-86-1
Na-EDTA	Astral Scientific	Cat#BIOEB0185
L-arginine-HCl	Sigma Aldrich	Cat#1119-34-2
Oxidized glutathione	Sigma Aldrich	Cat#64376
Reduced glutathione	GoldBio	Cat#64376
PMSF	Sigma Aldrich	Cat#10837091001
Ni-NTA resin	Qiagen	Cat#30410
HEPES-HCl	Sigma Aldrich	Cat#H4034
EndoH	New England Biolabs	Cat#P0702S
PEG 3350	Sigma Aldrich	Cat#202444
Tacsimate	Hampton Research	Cat# HR2-825
Tri-sodium citrate	Merck	Cat#1.06448.0500
P20	Cytiva	Cat#BR100054
Gentle Ag/Ab elution buffer	ThermoScientific	Cat#21027
Qubit Machine	Life Technologies	N/A
MiSeq Instrument	Illumina	N/A
Critical commercial assays		
EasySep Human NK Cell Enrichment Kit	Stemcell Technologies	Cat#19055
Cytofix/Cytoperm Plus kit	BD Biosciences	Cat#555028
Fugene6	Promega	Cat#E2691
DNAeasy Blood and Tissue DNA extraction kit	Qiagen	Cat#69506
QBit™ 1X dsDNA HS Assay Kit	ThermoFisher	Cat#Q33230
QBit™ 1X dsDNA BR Assay Kit	ThermoFisher	Cat#Q33265
MIA FORA NGS HLA MFlex 11 high-throughput kit	Immuncor	Cat#SR-800-00534-96
Deposited data		
LIFT cohort targeted KIR and HLA sequence reads	This paper	https://doi.org/10.7910/DVN/TRMTCT
PNG targeted KIR and HLA sequence reads	This paper	https://doi.org/10.7910/DVN/JA0U1Z
LIFT cohort HLA class I CDS alleles	This paper	GenBank# MH301276-78
LIFT cohort KIR3DL1 CDS alleles	This paper	GenBank# MH938271-97
KIR3DL1/HLA/peptide complex structural data	This paper	PDB# 9BL2-6, 9BL9, 9BLA
KIR3DL1*001/HLA-A*24:02/NEF structural data	Saunders et al.[48]	PBD: 7K80
IPD-IMGT/HLA, v3.25.0	Robinson et al.[92]	https://www.ebi.ac.uk/ipd/
IPD-KIR v2.13	Robinson et al.[51]	https://www.ebi.ac.uk/ipd/
HLA class I genotypes from the 13th IHWG	Mack et al.[93]	https://ftp.ncbi.nlm.nih.gov/pub/mhc/mhc/Final%20Archive/IHWG/Anthropology/
1000 Genomes Project	Byrska-Bishop et al.[94]	https://www.internationalgenome.org/
Simons Genome Diversity Project	Mallick et al.[95]	https://www.simonsfoundation.org/simons-genome-diversity-project/
Oceanian Genome Variation Project	Quinto-Cortes et al.[49]	N/A
MEGA data from 297 PNG individuals	Bergström et al.[50]	N/A
Māori KIR3DL1/S1 and HLA class I allele frequencies	Nemat-Gorgani et al.[27]	N/A

(*Continued on next page*)

Continued

REAGENT or RESOURCE	SOURCE	IDENTIFIER
Ga-Adangbe KIR3DL1/S1 and HLA class I frequencies	Norman et al.[96]	N/A
Nama and Khomani KIR3DL1/S1 and HLA class I frequencies	Nemat-Gorgani et al.[97]	N/A
Yucpa KIR3DL1/S1 and HLA class I frequencies	Gendzekhadze et al.[98]	N/A
Chinese Southern Han KIR3DL1/S1 and HLA class I frequencies	Deng et al.[99]	N/A
Europeans from USA KIR3DL1/S1 and HLA class I frequencies	Amorim et al.[100]	N/A
Malay KIR3DL1/S1 and HLA class I frequencies	Tao et al.[101]	N/A
1000 Genomes Project KIR3DL1/S1 genotypes	Norman et al.[102]	N/A
KIR3DL1/S1 frequencies, multiple populations	Norman et al.[25]	N/A
Native South American KIR3DL1/S1 allele frequencies	Vargas et al.[103]	N/A
KIR3DL1/S1 allele frequencies from 7 African populations	Nemat-Gorgani et al.[104]	N/A
Experimental models: Cell lines		
Human 721.221 cells	Laboratory of Peter Parham; Shimizu and DeMars[105]	N/A
Human 721.221 cells expressing specified HLA-A, -B or -C allele	Laboratory of Andrew Brooks; Saunders et al.[26,48,106]; Laboratory of Peter Parham; Saunders et al.[106]	N/A
293T cells	ATCC	Cat#CRL-3216
Jurkat cells	Laboratory of James McCluskey; Macdonald et al.[107]	N/A
Expi293F™ cells	ThermoFisher	Cat#A14527
Expi293F™ GnTI cells	ThermoFisher	Cat#A39240
Oligonucleotides		
Mutagenesis primers	This paper (Bioneer Pacific)	See Table S4
Recombinant DNA		
Codon-optimized HLA-B*51:01 construct	GeneArt Strings	N/A
pcDNA3.1(-) Mammalian Expression Vector	Invitrogen	Cat#V79520
KIR3DL1*001/*005 CD3ζ constructs	O'Connor et al.[108]	N/A
RSV.5neo.B2705	Laboratory of James McCluskey; Williams et al.[109]	N/A
pET-30 vector	Studier and Moffatt[110]	N/A
pHLSec Mammalian Expression Vector	Novagen	Cat#99845
Software and algorithms		
R version 4.1.1, 4.3.1	r-project.org	N/A
PING	Marin et al.[111]	https://github.com/Hollenbach-lab/PING
PONG	Harrison et al.[112]	https://github.com/NormanLabUCD/PONG
NGSengine 1.7.0	GenDX	https://www.gendx.com/
STRUCTURE	Falush et al.[113]	https://web.stanford.edu/group/pritchardlab/structure.html
Mega 6.0	Tamura et al.[114]	https://www.megasoftware.net/
PLINK2	Chang et al.[115]	https://www.cog-genomics.org/plink/2.0/

(*Continued on next page*)

Continued

REAGENT or RESOURCE	SOURCE	IDENTIFIER
KING version 2.2.2	Manichaikul et al.[116]	https://www.kingrelatedness.com/
HIBAG v1.36.4	Zheng et al.[117]	https://bioconductor.org/packages/release/bioc/html/HIBAG.html
EAGLE	Taliun et al.[118]	https://alkesgroup.broadinstitute.org/Eagle/downloads/
Generic Mapping Tools (GMT)	Wessel and Smith[119]	https://www.generic-mapping-tools.org/download/
ADMIXTURE v1.3.0	Alexander et al.[120]	https://dalexander.github.io/admixture/download.html
pong v1.5	Behr et al.[121]	https://github.com/ramachandran-lab/pong
RFMix v2.03	Maples et al.[122]	https://github.com/slowkoni/rfmix
SHAPEIT v4.2.2	Delaneau et al.[123]	https://odelaneau.github.io/shapeit4/
Bcftools 1.7	Danecek et al.[124]	https://samtools.github.io/bcftools/
MEGA v11.0.13	Tamura et al.[125]	https://www.megasoftware.net/
PAML v4.8	Yang[126]	http://abacus.gene.ucl.ac.uk/software/paml.html
Picardtools v2.27.5	http://broadinstitute.github.io/picard	N/A
Admixtools v7.0.2	Patterson et al.[54]	https://github.com/DReichLab/AdmixTools
Arlequin v3.5.2	Excoffier et al.[127]	https://cmpg.unibe.ch/software/arlequin35/Arl35Downloads.html
VCFtools v0.1.15	Danecek et al.[128]	https://vcftools.github.io/index.html
Selscan v1.2.0	Szpiech and Hernandez[129]	https://github.com/szpiech/selscan
XDS	Kabsch[130]	https://xds.mr.mpg.de/
Aimless (CCP4i program suite)	Collaborative Computational Project[131]	https://www.ccp4.ac.uk/
Phenix	Phenix project - Lawrence Berkeley Laboratory. Adams et al.[132]	https://phenix-online.org/
COOT	MRC Laboratory of Molecular Biology. Emsley and Cowtan[133]	https://www2.mrc-lmb.cam.ac.uk/personal/pemsley/coot/
PyMOL	Schrödinger, Inc.	https://pymol.org/2/
MX2 Beamline	Australian Synchrotron	N/A
BIAcore T200	GE Healthcare	N/A
GraphPad Prism v9	GraphPad	N/A
BD FACS Diva v8.0.3	BD Biosciences	N/A
BD Fortessa II or BD FACS Canto II	BD Biosciences	N/A
FlowJo v9.9.6 or 10.9.0	BD Biosciences	N/A
bioRender	biorender.com	Graphical abstract
Other		
S200 16/60 column	GE Healthcare	Cat#28989335
HiTrap-Q anion exchange chromatography	GE Healthcare	Cat#17115301
CM5 sensorchip	Cytiva	Cat#BR100530

EXPERIMENTAL MODEL AND STUDY PARTICIPANT DETAILS

Human Participants

First Nations Australian Donors

All experiments conformed to the National Health and Medical Research Council (NHMRC) of Australia code of practice and were approved by The University of Melbourne Human Research Ethics Committee (Applications #1441452.1 and #0931311.5) and the Human Research Ethics Committee of the Northern Territory Department of Health and Menzies School of Health Research (#HREC-2012-1928). Healthy, self-declared First Nations Australian volunteers were recruited from the Royal Darwin Hospital Outpatient clinic as part of the "Looking Into inFluenza T-cell immunity" (LIFT) cohort.[7] Written informed consent was obtained from all

donors. Median age was 45 years (interquartile range 30, 55) and 52% were male.[7] Per individual information on age and gender is not available and unlikely to affect the results of the gene sequencing or NK cell assays performed. Peripheral blood mononuclear cells (PBMC) were isolated from heparinized blood using Ficoll-Paque (GE Healthcare, Marlborough, MA, USA) density gradient centrifugation and resuspended in fetal calf or bovine serum (FCS/FBS; Gibco/ThermoFisher Scientific, Waltham, MA, USA) containing 10% DMSO for cryopreservation. Samples from other individuals were obtained from Australian Red Cross LifeBlood with approval from the University of Melbourne Human Research Ethics Committee (Project 1238243.2), with PBMC isolated from buffy coats and cryopreserved as above.

Papua New Guinea Donors

DNA was obtained from 645 Papuan individuals as described previously.[50] Briefly, samples were sourced from a library of samples collected in the 1980s in a series of collaborative projects between the Institute for Medical Research in Papua New Guinea, Liverpool School of Tropical Medicine, and the University of Oxford, UK. The samples were collected, following informed consent, to understand genetic differences between highland and lowland populations in relation to differential disease risk. The median recorded age was 23 years (interquartile range 17, 30) and 42.5% were male. All samples were collected at the time with regulatory approval from the Papua New Guinea Institute of Medical Research, and the Papua New Guinea Medical Research Advisory Council, and endorsed by the Public Health Department. Updated approval for contemporary genetic analysis was provided by the Institute for Medical Research in Papua New Guinea, and the Oxford Tropical Research Ethics Committee (OxTREC).

METHOD DETAILS

KIR and KIR-ligand nomenclature

The *KIR* locus varies in gene content from approximately six to 13 genes per haplotype.[16] Included are up to four genes encoding inhibitory receptors specific for HLA class I; KIR2DL1, 2DL2/3, 3DL1 and 3DL2. In turn a given HLA class I allotype may contain one of four distinct amino acid motifs that enables it to become a KIR ligand. Those HLA allotypes that do not have either of these motifs do not function as KIR ligands. The ligand motifs are A3/11 (carried by some HLA-A), Bw4 (some HLA-A and B), C1 (some HLA-B and C) or C2 (some HLA-C). KIR2DL1 is specific for $C2^{+}$HLA, 2DL2/3 for C1 and some C2, 3DL1 for Bw4, and 3DL2 for A3/11. KIR are named according to the number of external Ig-like domains (2D or 3D), which can bind to the ligand, and 'L' denotes 'long' cytoplasmic tail that can transmit a signal to inhibit cellular activity upon ligand binding. Throughout this manuscript, any unique DNA sequence that spans a coding region is considered a distinct allele. Those alleles that encode a unique protein sequence define an allotype.

High-resolution KIR and HLA allele genotyping

Genomic DNA from the 80 LIFT donors was prepared from PBMC, or granulocytes isolated after Ficoll separation of PBMC from whole blood, using the DNeasy Blood and Tissue DNA extraction kit (Qiagen, Hilden, Germany). DNA was quantified using a Qubit machine (Life Technologies, Carlsbad, CA, USA). *KIR* and *HLA class I* and *II* genes were analysed concurrently using high throughput sequencing, as described.[102] Sequencing was performed using a MiSeq instrument (Illumina) with V3 chemistry, and the sequencing read length was 2 x 300 bp. To determine the gene and allelic content of the *KIR* locus, sequenced reads were analysed using the Pushing Immunogenetics to the Next Generation (PING) pipeline.[102,111] The IPD-KIR database v2.13 was used as the source of reference sequences.[51] *HLA* alleles were determined using NGSengine 1.7.0 (GenDX, Utrecht, Holland). HLA typing of the additional donors used for NK cell experiments was performed by the Victorian Transplantation and Immunogenetics Service (Australian Red Cross LifeBlood). The KIR3DL1 subtype of these donors was initially identified from gDNA using a multiplex PCR[134] and confirmed by high resolution KIR typing as above.

Admixture analysis

A previous genome wide study of First Nations Australians identified admixture with Europeans.[28] To determine the contribution of this admixture to the high HLA diversity in First Nations Australians, we compared the distribution of *HLA-A* and *-B* alleles to those of other populations chosen to represent major world groups. We did not include *HLA-C* due to strong linkage disequilibrium (LD) with *HLA-B*. We examined admixture among the populations using the program STRUCTURE.[113] As additional data we used *HLA class I* genotypes of individuals obtained from the 13th Histocompatibility Workshop[93] (https://ftp.ncbi.nlm.nih.gov/pub/mhc/mhc/Final%20Archive/IHWG/Anthropology/), as well as Māori,[27] Ga-Adangbe,[96] Hadza,[104] and Khomani[97] individuals; thus 3,196 individuals were included from 32 populations (Table S2), representing five regions (Europe, Oceania, South East Asia, East Asia, and Sub-Saharan Africa). Using STRUCTURE,[113] the 3,196 individuals were assigned to pre-determined *K* clusters (K=2 to K=5), where individuals may have contributions from more than one cluster.

The STRUCUTRE analysis showed the First Nations Australian *HLA class I* genotypes cluster with other Oceanian populations but are distinguished from them by having a proportion of genetic ancestry shared with Europeans (Figure S1). This finding focused on the *HLA class I* genes is thus consistent with the independent genome-wide study.[28] Restricting our analysis to European, Oceanian and Southeast Asian groups revealed that up to 39% of the sampled First Nations Australians have >50% and 33% have >75% European genetic ancestry detected in their *HLA class I* genes (Figure S1). A separate, allele specific, analysis permitted inclusion of *HLA-C*. Analyzing only alleles observed in more than one individual, 9/15 *HLA-A*, 11/28 *HLA-B* alleles, and 6/17 *HLA-C* were

identified to originate from Europeans (Figure S1). One allele of HLA-A (*A*34:01*), six alleles of HLA-B (*B*13:01, *15:21, *15:25, *27:04, *27:06, *56:02*) and one allele of HLA-C (**15:09*) are present in Papua New Guineans, but not Europeans, indicating their likely Oceanian origin for First Nations Australians. A further three alleles (*B*40:06, *48:01, *55:02*) were identified in East Asians, but not Papua New Guineans or Europeans. As East Asian admixture is not detected in First Nations Australians from Northern Australia,[28] these three alleles also likely arrived in Australia during the migration from Papua New Guinea.

Analysis of the ten most frequent First Nations Australian *HLA class I* haplotypes identified six that were observed also in Papua New Guineans and not Europeans, and three in Europeans but not Papua New Guineans (Figure S1). Although this analysis has low sensitivity, the overall admixture proportions and geographic *HLA* allele distributions are consistent with previous studies.[28,44,135] Together, these results show that although the *HLA class I* allele distribution of First Nations Australians from the North Top End region is closely related to other Oceanian populations, diversity has been increased through admixture with Europeans.

Novel Allele Confirmation

For confirming novel *KIR* alleles, individual exons of the *KIR* genes were amplified from genomic DNA and subjected to Sanger sequencing using primers and protocols as described.[96] The IPD-KIR database v2.13 was used as the source of reference sequences.[51] For confirming *HLA* allele sequences, HLA-A, -B, -C genes were amplified using long-range PCR reactions from the MIA FORA NGS high-throughput kit (Immucor, Inc., Norcross, GA, USA), performed and analyzed according to the manufacturer's protocol. The IPD-IMGT/HLA database v3.25.0 was used as a source of reference sequences.[92] All novel allele sequences were deposited in GenBank and IPD,[51] and the accession numbers are given in Table S1D.

Phylogenetic analysis

Neighbour-joining phylogenetic analyses of the coding determining sequence (CDS) of the external domains (cytoplasmic tail excluded) were generated, with 500 bootstrap replicates, using the Tamura-Nei model with pairwise deletion, using Mega 6.0.[114]

Population comparisons

To measure *HLA* and *KIR* diversity across populations (Figure 1) we used representative groups that were previously genotyped to the same high resolution as this study; West Africans from Ghana,[96] Nama and Khomani Southern Africans,[97] Yucpa Amerindians,[98] Chinese Southern Han,[99] Europeans from USA,[100] Malay,[101] and Māori.[27] The number of distinct alleles present in 75 randomly selected individuals was counted, and the process was repeated for 1,000 permutations with replacement.

Worldwide distribution of KIR3DL1 ligands

To determine the relative proportions of HLA-A and -B allotypes carrying ligands for 005-lineage and 015 lineage KIR3DL1 we used HLA allele frequency data from the same populations as above. Those allotypes carrying the Bw4 motif of residues 77-83 (N/D77, I/T80, A/L81, L82, R83),[13] were divided into those that bind preferentially to 005-lineage KIR3DL1 and those that also bind to 015-lineage KIR3DL1. A threshold of 25% maximum binding as previously determined (Figure 2C from Saunders et al.[26]) was used to distinguish these characteristics. For rare allotypes present in the data set but not previously tested, the binding pattern of the closest aligning allotype was used (e.g. HLA-A*24:03 was given the same value as A*24:02). HLA-A*25 and B*13 have not been shown as effective ligands for KIR3DL1[23,26,48] and were counted as non-binders for this analysis.

Worldwide distribution of KIR3DL1 alleles

KIR3DL1 allele frequencies were obtained from previously sequenced 1000 Genomes individuals,[102] and other worldwide populations,[25,99–101,103,104] including Māori and Polynesians[27] and First Nations Australians and Papua New Guineans (this study). *KIR3DL1* allele frequencies from additional Oceanian populations were determined through imputation, as described below.

Genome-wide array data

We analyzed previously generated genome-wide array data from 913 Oceanian individuals from the Oceanian Genome Variation Project (OGVP)[49] and an additional set of 297 Papua New Guinea individuals,[50] genotyped using the Multi-Ethnic Genotyping Array (MEGA) array. We used PLINK2[115] to exclude individuals or SNPs having genotype missingness > 10%, and SNPs having minor allele frequency < 1%. We also removed related individuals (2nd degree or more), as estimated using KING version 2.2.2.[116] The final Oceanian dataset after quality control filtering contained 471,417 SNPs and 1,108 unrelated individuals. Of these, 345 individuals overlapped with the set of individuals sequenced as described above. The Oceanian dataset was then merged with reference populations from the phase3 1000 Genomes Project[136]: Utah residents (CEPH) with Northern and Western European ancestry (CEU), Han Chinese in Beijing, China (CHB), Kinh in Ho Chi Minh City, Vietnam (KHV), and Yoruban from Idaban, Nigeria (YRI), available in http://ftp.1000genomes.ebi.ac.uk/vol1/ftp/release/20130502/. The final merged dataset contained 463,750 SNPs and 1,517 individuals.

HLA and KIR imputation

HLA alleles were imputed from the genome-wide array data using HIBAG version 1.36.4,[117] using default parameters and the pre-trained Asian model for the human genome build GRCh37/hg19, available at https://hibag.s3.amazonaws.com/download/hlares_param/Asian-HLA4-hg19.RData. To assess the accuracy of the imputation, we compared with those individuals who had been

genotyped using other means: Papua New Guinea (345 sequenced as described above), 1000G CHB and KHV (https://ftp.1000genomes.ebi.ac.uk/vol1/ftp/data_collections/HLA_types/). Accuracy, defined as the number of correct calls per sample divided by the size of the dataset (2N), was 95.81%.

KIR3DL1/S1 alleles were imputed from the genome-wide array data using PONG.[112] We first performed SNP imputation using the Michigan imputation server, where the data was phased using EAGLE.[118] Only high-quality imputed variants were kept (Rsq > 0.3). The published PONG training models did not include the *3DL1*114* allele. We therefore trained a new model using 150 Papua New Guinea, 60 CHB and 40 KHV individuals, and tested the model with 153 Papua New Guineans, 20 CHB, and 24 KHV individuals. This model has an accuracy of 70.05%. Specifically, for *3DL1*114* we prioritized a high specificity (97.72%), to avoid reporting false positives and overestimating its frequency. The estimates of *3DL1*114* allele frequency are thus conservative.

Mapping allele distributions

Relative allele frequencies were plotted using the Generic Mapping Tools (GMT).[119] Available point values were used to estimate two-dimensional frequency distributions with *blockmean* and *surface* functions as previously described.[56] We used the *psmask* function to clip unreliable map areas, considering reliable only those grid cells within a 1,300 km radius of a data point.

Genetic ancestry analyses of Oceanian dataset

To analyze the genetic structure across our Oceanian dataset, we performed ADMIXTURE analysis, using the merged genome-wide array data. LD pruning was applied using PLINK2,[115] with a window size of 200kb, step size of 50 SNPs and r^2 threshold of 0.5, resulting in 247,344 unlinked SNPs. ADMIXTURE version 1.3.0[120] was run in unsupervised mode using ten different iterations with random seeds. The major mode for the ten independent runs was identified using pong version 1.5.[121] As shown in Figure S2A, at K=5, there was a component maximized in the YRI population (dark red: ''African-related''), others maximized in CEU (orange: ''European-related''), CHB (beige: ''East Asian – related''), Highlanders from Papua New Guinea (blue: ''Papuan-related''), and Polynesian populations (purple: ''Polynesian-related'').

After estimating the global genetic ancestries with ADMIXTURE, we used RFMix version 2.03[122] to perform local ancestry inference. Data was phased using SHAPEIT version 4.2.2,[123] with default parameters. RFMix was run with one Expectation-Maximization iteration and four reference panels. As reference, we used the KHV and CHB (n=202) for the East Asian ancestry proxy, CEU (n=99) for the European proxy, the Papuan reference panel included those individuals with >99% of ''Papuan-related'' component in the ADMIXTURE analysis (n=100), and the Polynesian panel included individuals with >90% of ''Papuan-related'' component (n=80). We only kept windows having a marginal probability >90%. Correlations between global ancestry proportions inferred from ADMIXTURE K=5 and RFMIX were higher than 0.94 for all ancestries, and higher than 0.98 for both the Polynesian and Papuan-related components (Figure S2B).

Divergence time estimation

Divergence times between *KIR3DL1*114* and **005* and **015* gene sequences (13,781 bp) were estimated. Bcftools 1.7 consensus[124] was used to obtain the *KIR3DL1* gene sequences from short-read sequencing data obtained from four *KIR3DL1*114* homozygous Papuan individuals. We used the ClustalW algorithm of MEGA 11.0.13[125] to align these sequences with one *KIR3DL1*015* and one *KIR3DL1*005* sequence (GenBank ID GU182342.1 and GU182344.1, respectively) and constructed a maximum likelihood phylogenetic tree with default parameters. Divergence time was estimated using mcmctree of PAML v4.8,[126] using the same parameters as,[137] except the 'RootAge', which was set to a maximum of 6.5mya, corresponding to the split of chimpanzee and human.[138] The acceptance proportions, times and rates were stable throughout the MCMC runs. Analysis convergence was further explored running the analysis 10 times with different random seeds, showing similar values for the ten sets of posterior times.

Denisovan introgression: D-statistics

To infer Denisovan introgression, we used genome-wide chromosome 19 SNP data from the 1000G Yoruban from Idaban, Nigeria (YRI, *KIR3DS1*$^-$ individuals, N= 104),[94] the Denisovan genome (http://cdna.eva.mpg.de/denisova/VCF),[33] the predicted ancestral sequence for *Homo sapiens* derived from a multiple alignment of seven primate genomes (available in https://ftp.ensembl.org/pub/release-76/fasta/ancestral_alleles), as well as the 14 KHV individuals, and four *KIR3DL1*114*$^+$ homozygous individuals described above. The Denisovan genome was lifted over from hg19 to the GRCh38 reference using Picardtools v2.27.5 LiftoverVCF (http://broadinstitute.github.io/picard). After keeping only common SNPs from the *KIR2DL4-3DL1* genomic region, 65 SNPs remained in the merged dataset. A similar approach was used for HLA-A alleles, using OGVP array data. Here in each case the allele sequence +/- 500kbp was used.

D-statistics, which measure the degree of allele sharing across populations, were calculated using Admixtools 7.0.2[54] in the form of D-statistic (W, YRI, Denisovan genomic sequence, Ancestral sequence), where W corresponds to individuals carrying *KIR3DL1*114*, **005*, or **015*. Significant introgression from Denisovan to *KIR3DL1* haplotypes was considered when D-score > 0 and Z-score > 3.

A recombination hotspot divides the *KIR* locus into two regions, termed 'centromeric' and 'telomeric' according to their orientation.[139] All four *KIR3DL1*114* homozygous Papuan individuals we sequenced have the following telomeric *KIR* haplotype: *2DL4*028∼3DL1*114∼2DS4*019∼3DL2*002*, which is the most common haplotype in Papuan *3DL1*114*$^+$ individuals (Figure 2D). To infer the length of the introgressed haplotype, we performed the D-statistic test as described above, but progressively including

KIR genes from the telomeric and centromeric regions (*2DL4-3DL1-2DS4-3DL2*, and *2DL1-2DL2/3-2DS2-3DL3*, respectively), until the number of BABA SNPs stopped increasing (SNPs where the allele is shared between the target *3DL1*114* and Denisovan genome).

To test if the *KIR3DL1*114* carrying haplotype is a result of incomplete lineage sorting instead of archaic gene flow into modern humans, we applied the following formula[55]: $P = 1 - gammaCDF\left(H, shape = 2, rate = \frac{1}{L}\right)$; where P is the probability that a haplotype of a particular length (H) is shared between Oceanians and Denisovans due to incomplete lineage sorting; and $L = 1/(r \times t)$, where r is recombination rate per generation per base pair (bp) (mean recombination rate around *KIR2DL4* ~ *KIR3DL2* is: 2.91×10^{-8}; from the HapMap recombination map[140,141]) and t is the number of generations since the Denisovan and modern human divergence (300×10^3 years ago / 25 years per generation[55]). After applying the formula, we found that the probability of a haplotype of length 62,276 bp present in modern Oceanians due to incomplete ancestral lineage sorting is 8.78×10^{-9}, which supports the alternative hypothesis of being in modern Oceanians due to Denisovan introgression.

Statistical tests for positive selection

To examine the frequency distribution of *HLA* alleles, we used Arlequin version 3.5.2[127] and R version 4.3.1 to calculate the Ewens-Watterson F-statistic for homozygosity and Hardy Weinberg Equilibrium (HWE) chi-squared tests. We also calculated the nucleotide diversity (π) in 100 bp windows from genome-wide array data using VCFtools version 0.1.15.[128] Although π may be underestimated using SNP array compared to sequencing data,[142–144] the results are consistent with *HLA-A*24:02* carrying haplotypes having lower diversity than the two other *HLA-A* alleles common in the geographic region.

To test for evidence of recent positive selection of HLA-A*24:02, we computed the iHS statistic (integrated haplotype score[145]). We used publicly available whole genome phased sequences of 15 Papua New Guinea individuals from the Simons Genome Diversity Project (SGDP,[95] available at: https://sharehost.hms.harvard.edu/genetics/reich_lab/sgdp/phased_data2021/). We used these results because SNP coverage within the *HLA-A* region in the MEGA array used for OGVP is insufficient to correctly construct the ancestral and derived haplotypes needed for the iHS calculation. We assigned the ancestral and derived state for each variant based on the ancestral state information from the 1000G phase3 data.[136] iHS calculation and normalization across frequency bins of the unstandardized iHS were performed using selscan version 1.2.0[129] with default parameters. To validate that the selection signal observed is due to the *HLA-A*24:02*, we imputed the *HLA-A* alleles in these individuals using HIBAG version 1.36.4,[117] and identified 7 and 5 *HLA-A*24:02* homozygotes and heterozygotes, respectively. All the SNPs within the iHS positive peak within the *HLA-A* and flanking region have derived alleles in *HLA-A*24:02*$^+$ individuals, confirming the positive selection signal is related to the haplotype of *HLA-A*24:02*.

Purification and expansion of NK cells

PBMC samples were thawed, and NK cells isolated using the EasySep™ Human NK Cell Enrichment Kit, according to the manufacturer's instructions (Stemcell Technologies Vancouver, Canada). Primary NK cells were rested overnight in complete media before use in *ex vivo* analyses. Expanded NK cells were prepared by incubating with irradiated feeder cells and HLA-G-expressing 721.221 cells in the presence of 100 U/mL rhIL2 (Miltenyi) and 1.5 ng/mL PHA (Gibco/ThermoFisher Scientific) in complete media as previously described.[26] All feeder cells were isolated from a single independent donor (donor CM: *HLA-A*32:01, A*33:01, B*07:05, B*44:03, C*03:03, C*0701; KIR3DL1*004/KIR3DS1*013*). The complete media was RPMI 1640 supplemented with 7.5mM HEPES, 2 mM L-Glutamine, 150 μM non-essential amino acids, 76 μM 2-ME, 150 μg/ml streptomycin and 10% FBS (In Vitro Technologies, Noble Park North, VIC, Australia) and 100 U/mL rhIL2 (Miltenyi, Bergisch Gladbach, Germany).

Target cell lines

The B-lymphoblastoid cell line 721.221,[105] which expresses no endogenous HLA-A, -B or -C[105], transfected with HLA-A*23:01, A*24:02, A*25:01, A*32:01, B*08:01, B*13:01, B*27:05, B*44:02, B*57:01, B*58:01, C*04:01 or C*07:02 have been described previously.[26,48,106] Codon optimised HLA-B*51:01 constructs were purchased (GeneArt Strings, ThermoFisher Scientific) and cloned into pcDNA3.1(-) using EcoRI and BamHI. HLA-B*27:04 and B*27:06 were generated in the RSV5neo[109] plasmid via sequential site directed mutagenesis from HLA-B*27:05 using primers listed in Table S4. Plasmid constructs were electroporated into 721.221 cells at 200V and 975μF and placed under geneticin selection as previously described.[26] Transfected cells were sorted for HLA class I expression following staining with pan-HLA class I specific W6/32 monoclonal antibody; cells were stained using unconjugated W6/32, and counterstained using FITC conjugated antibody specific for IgG. The geometric mean fluorescence intensity (gMFI) of HLA class I expression for each of the cell lines was determined (Table S4). They were maintained in RPMI 1640 media (Media Preparation Unit, University of Melbourne, Australia) supplemented as above, but without IL2. Expression of specific HLA allotypes was confirmed by staining with mAb specific for the Bw4 epitope (RM7.9.63[88]), HLA-B27 (ME1[89]) or the B17 (B*57 and B*58) serotype (3E12[90]), followed by anti-mouse IgG-FITC, or HLA-A24/A2 (One Lambda) followed by anti-mouse IgM-PE. The HLA-C controls were stained using a directly conjugated antibody specific for HLA-C/E (DT9; PE; BD Pharmingen).

NK cell assays

NK cells were incubated with HLA class I-transfected or non-transfected target cells at a 1:2 (*ex vivo* NK cells) or 1:1 (expanded NK cells) effector:target ratio for 1 hour at 37°C in the presence of anti-CD107a-PECy5 (H4A3; BD Biosciences, San Jose, CA, USA). We

used CD107a as a measurement of degranulation and thus a proxy for NK cell killing of target cells[146] and IFNγ as a marker for NK cell activation. Monensin (GolgiStop; BD Biosciences) was added according to the manufacturer's recommendations and following a further four hours of incubation, cells were washed and cell surface stained. The cells were stained for the following markers: KIR3DL1 (NKB1 (DX9), FITC; BD Biosciences), KIR2DL2/L3/S2 (GL183, PE-Cy5.5; Beckman Coulter, Brea, CA, USA), KIR2DL1/S1 (EB6B, PE-Cy7; Beckman Coulter), LILRB1 (HP-F1, APC; eBioscience/ThermoFisher), and NKG2A (Z199, PE; Beckman Coulter). *Ex vivo* NK cells were further stained with Live/Dead Aqua (LifeTechnologies/ThermoFisher), CD56 BV786 (BD Biosciences) and CD3 UCHT1, PacificBlue (BioLegend, San Diego, CA, USA). Expanded NK cells were further stained with eBioscience™ Fixable Viability Dye eFluor™ 780 (Invitrogen/ThermoFisher), CD56 (NCAM16.2, BV421: BD Biosciences) and CD3 (SK7, APC-Cy7, BD Biosciences). Cells were fixed and permeabilized (Cytofix/Cytoperm kit; BD Biosciences), stained for IFNγ (B27, AF700; BD Biosciences) and acquired using a BD LSRFortessa flow cytometer, with FACS DIVA software (Version 8.0.3).

KIR3DL1$^+$ NK cells were identified by gating on live NK cells (CD56$^+$CD3$^-$CD14/19$^-$). NK cells expressing other inhibitory receptors for HLA class I were excluded by selecting those negative for NKG2A, KIR2DL2/3 and KIR2DL1/S1. NK cell degranulation (CD107a[146]) and IFNγ production was assessed using FlowJo software version 9.9.6 (BD Biosciences, USA). The gating strategy is shown in Figure S3A. To account for any differences in the maximal cytokine production profiles between individuals, the maximum percentage (% of max of IFNγ or CD107a) for each donor was normalized to those values obtained from KIR3DL1$^+$ NK cells incubated with the parental 721.221 cell line. Showing that the inhibition is specific to KIR3DL1, upregulation of CD107a or IFNγ was not significantly diminished in NK cells expressing only KIR2DL2/3 or KIR2DL1/S1 from the same donors, assessed in parallel (Figure 3C). Secondly, target cell induced degranulation was restored by blocking the interaction using the KIR3DL1-specific monoclonal antibody DX9 (Figure S3C). Also included in the expanded NK cell assays were HLA-A*25:01 (Bw4$^+$), HLA-C*07:02 (C1), neither of which are recognised by KIR3DL1.[48]

Jurkat-KIR cellular reporter and activation assay

Constructs encoding KIR3DL1*001 or *005 linked to CD3ζ in the GFP$^+$ pMIGII[91] vector have been described previously.[108] The KIR3DL1*015+CD3ζ construct was generated by sequential site directed mutagenesis from the KIR3DL1*001+CD3ζ construct (Table S4). Further mutagenesis was then performed to generate KIR3DL1*086, *114, *001L166F and *015L166F constructs. Each KIR3DL1+CD3ζ construct was transduced into the Jurkat CD4$^+$ T cell line, using retrovirus.[147] Briefly, 4μg pMIGII.-KIR3DL1+CD3ζ along with 4μg pPAM-E[91] and 2μg pVSVG[91] was transfected into 293T cells using Fugene6 as per manufacturer's instructions (Promega) and cultured in DMEM media with 10 % FBS and supplements. Twenty-four hours after transfection, supernatant was collected, filtered, and used to resuspend freshly pelleted Jurkat[107] cells. Media transfer was performed twice daily for six days and transduced Jurkat cells were then selected by sorting for GFP and KIR3DL1 surface expression using anti-Human CD158e/k-PE, clone 5.133 (Miltenyi Biotec). Stably transduced Jurkat cells were maintained in RPMI (Gibco/ThermoFisher) supplemented as described above for NK cells, but without IL-2. For activation assays, transduced Jurkat cells expressing specific KIR3DL1+CD3ζ allotypes were incubated with equal numbers of HLA-transfected or non-transfected 721.221 targets for eight hours at 37°C. Cells were then washed, stained for CD69 (clone FN50, PE; BD Biosciences) and fixed. Samples were analysed using a BD FACSCantoII and the expression of CD69 on GFP$^+$ transduced Jurkat cells was assessed using FlowJo software Version 10.9.0 (BD Biosciences).

Protein expression and purification

The heavy chains (residues 1-276) of HLA-A*24:02, C*05:01 and B*57:03 were expressed into inclusion bodies in *E.coli* BL21 (DE3) from the pET-30 vector[110] and refolded in the presence of full-length β2-microglobulin (residues 1-99) and the relevant peptides, and purified as described previously.[24,148] Briefly, the HLA-peptide complexes were refolded by dilution into refolding buffer (5 M Urea, 100 mM Tris-HCl (pH 8), 2 mM Na-EDTA, 400 mM L-arginine-HCl, 0.5 mM oxidized glutathione, 5 mM reduced glutathione, 1 mM PMSF) and stirred for 72 h at 4°C. Then, the refolded solutions were dialyzed in 10 mM Tris-HCl pH 8.0 and purified by anion exchange on a diethylaminoethylcellulose column, followed by gel filtration (S200 16/60 column, GE Healthcare) and HiTrap-Q anion exchange chromatography (GE Healthcare).

Residues spanning from 1 to 299 of KIR3DL1*001, *005, *015 (with an N-terminal 6xHis), and *086, *114, *086-166L and *114-166L (with a C-terminal 6xHis), with secretion tags, were cloned into the pHLSec mammalian expression vector (Novagen) and expressed in Expi293F™ cells (Thermo Fisher) for Surface Plasmon Resonance (SPR) experiments and Expi293F™ GnTI- cells for structural studies. Soluble proteins were purified after 7 days from the culture media using Ni-NTA resin (Qiagen) and further purified by size exclusion chromatography using an S200 16/60 column (GE Healthcare). For SPR studies, purified KIR proteins were concentrated in a buffer composed of 10 mM HEPES-HCl (pH 7.4) and 300 mM NaCl. For crystallization trials, KIR proteins were concentrated to 15 mg/mL in 10 mM Tris-HCl (pH 8) and deglycosylated overnight at 4°C with EndoH (New England Biolabs).

Crystallisation and structure determination

All KIR3DL1/HLA/peptide complexes described were combined at 1:1 molar ratio and crystallized at 294 K using the hanging-drop vapour-diffusion method from a solution comprising 14%-18% PEG 3350, 2% Tacsimate pH 5 and 0.1 M tri-sodium citrate pH 5.6. Crystals were equilibrated in crystallization solution with 35% PEG 3350 added as cryoprotectant and then flash-frozen in liquid nitrogen. Crystallographic diffraction data were collected at the MX2 beamline (Australian Synchrotron). The data were processed with the program XDS[130] and scaled using Aimless from the CCP4 suite of program.[131] The crystal structures were determined by

molecular replacement using PHASER with KIR3DL1*001 and HLA-A*24:02 (PDB 7K80) as search models. Refinement of the models was carried out with iterative rounds of refinement in Phenix[132] and manual building in COOT.[133] Data collection and refinements statistics are summarised in Table S5. Data were deposited in the Research Collaboratory for Structural Bioinformatics PDB with the accession codes 9BL2-6, 9BL9 and 9BLA. KIR3DL1*001 bound to HLA-A*24:02-NEF was described previously (7K80).[48]

Surface Plasmon Resonance

SPR experiments were conducted using a BIAcore T200 instrument (GE Healthcare Life Sciences) as previously described.[61] Briefly, the HLA-peptide complexes were captured, to a density of ~800 resonance units, on a CM5 sensorchip (Cytiva) by immobilization of the anti-HLA mAb W6/32 (generated in-house).[87] KIR3DL1*001, *005, *015, *086, *114, *086-166L and *114–166L were serially diluted (0–150 μM) and injected (60 s association, 180 s dissociation) over the chip at a flow rate of 5 μl/min at 298 K in a buffer composed of 10 mM HEPES-HCl (pH 7.4), 300 mM NaCl and 0.005% surfactant P20. Chip surfaces were regenerated between each analyte injection using Gentle Ag/Ab elution buffer (Thermo Scientific). Resulting sensograms were subtracted against a reference flow cell coupled with W6/32 in the absence of HLA ligand capture. Binding affinities were determined by equilibrium analysis by implementing the one-site specific binding model using GraphPad Prism v9. All data are representative of two independent experiments, each conducted using duplicate samples. To allow direct comparison, for affinity curves the K_D fold change was normalised based on the Bmax, where Bmax was equated to 1000RU for each KIR3DL1/HLA experiment. Data are represented as mean ± SEM.

QUANTIFICATION AND STATISTICAL ANALYSIS

The description of all statistical analyses is in the corresponding figure legends. For each test, the alternative hypothesis was two-sided. Bar plot error bars represent mean ± standard deviation. Number of bootstraps, permutation resamples, and independent experimental replicates are indicated in the figure legends. P-values < 0.05 or Z-scores > |3| were considered significant. All multiple test correction was performed using the Bonferroni method. Plots and statistical tests were performed using R version 4.1.1.[149] or GraphPad Prism v9.

CellPress
OPEN ACCESS

Supplemental figures

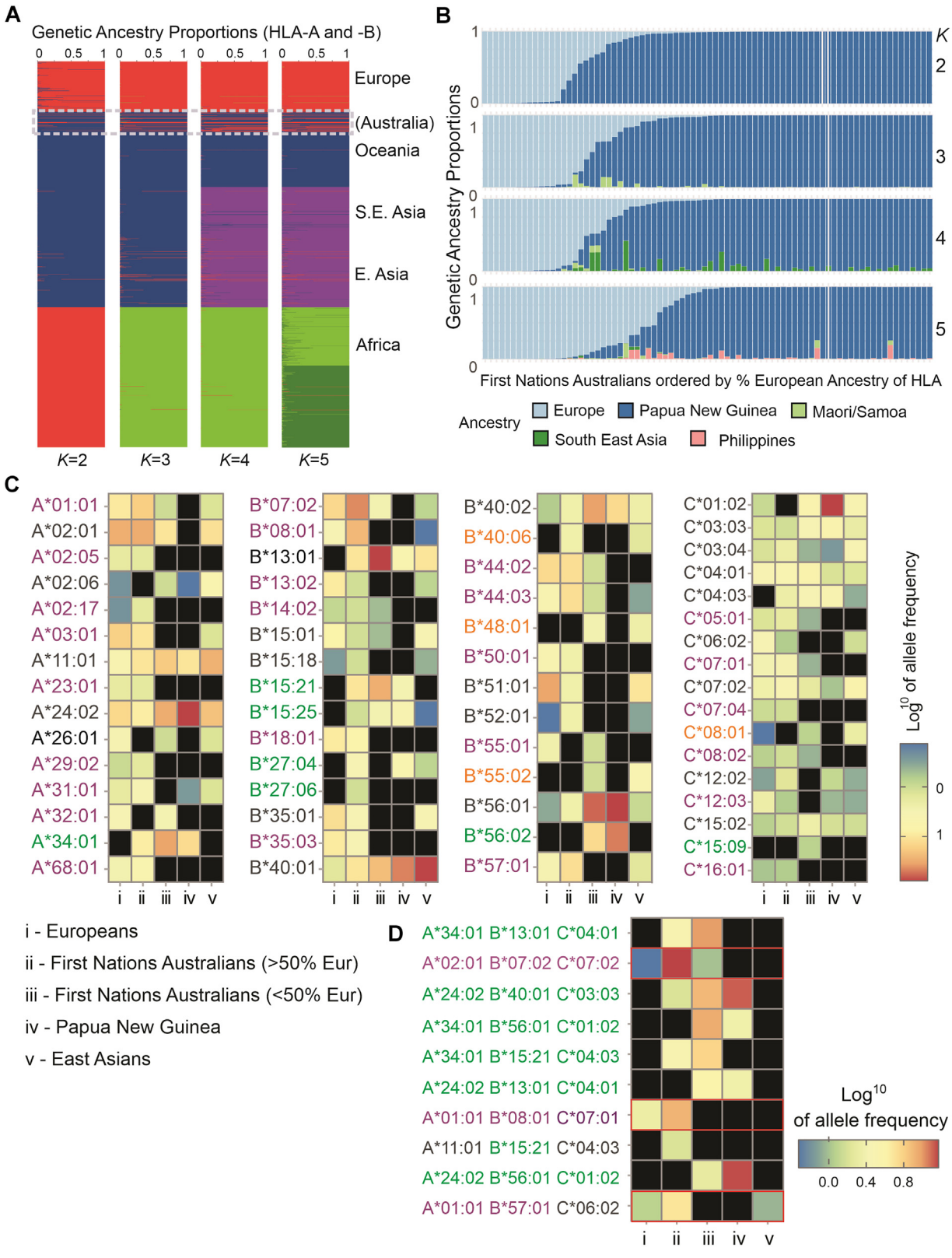

(legend on next page)

Figure S1. Ancestry proportions of *HLA class I* alleles and haplotypes, related to Figure 1

(A) Ancestry analysis using *HLA-A* and *-B* genotypes of representative populations (Table S2). *K* values at the bottom indicate the number of population clusters used for that analysis. Each horizontal line represents one individual, with colors indicating relative proportions of the *K* clusters. First Nations Australians are marked with a box outlined with gray dotted line. The other populations represent Europe, Oceania, Southeast Asia, East Asia, and Sub-Saharan Africa, as indicated at the right.

(B) Shows the genetic ancestry proportions estimated from *HLA-A* and *-B* genotypes of the 80 First Nations Australians. Here, the analysis is restricted to European, Oceanic, and Southeast Asian populations, and each vertical line represents one individual. Colors indicate relative proportions of the K components, and each of them is assigned to a population group (key at the bottom), where each component is maximized.

(C) *HLA-A*, *-B*, and *-C* alleles observed in >1 First Nations Australian are studied. Shown are the frequencies of those alleles observed in (Ci) Europeans, (Cii) First Nations Australians having >50% European-related ancestry in *HLA* (B), (Ciii) First Nations Australians having <50% European-related ancestry in *HLA*, (Civ) Papua New Guineans, and (Cv) East Asians. Colors depict the $\log_{10}$ frequencies as given in the key. Alleles absent from Papuans but present in Europeans and thus of likely European origin are indicated with purple text; those absent from Europeans are indicated with green text. Those alleles absent from Europeans and Papuans but present in East Asians are indicated in orange text. Any alleles present in both Europeans and East Asians are denoted European if frequency <1.5% in East Asians, and vice versa.

(D) For the ten most frequent *HLA class I* haplotypes observed in First Nations Australians (left), this shows the $\log_{10}$ frequency in Europeans (Di), First Nations Australians (Dii and Diii), Papua New Guineans (Div), and East Asians (Dv). Colors depict the frequencies as given in the key at the right. Green text indicates oceanic-descent haplotypes, and purple text indicates likely European-descent haplotypes. For two haplotypes (8 and 10) having inconclusive ancestries from the haplotype frequencies, the genetic ancestries of the component alleles derived in (C) are shown. Haplotypes of likely European origin are marked with a red box.

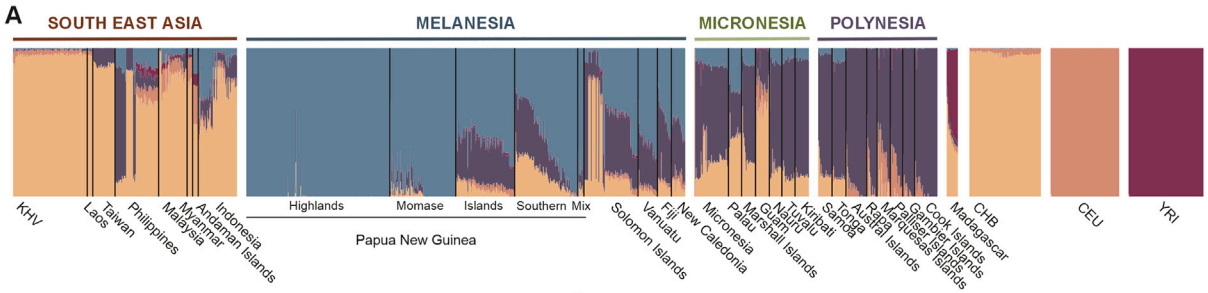

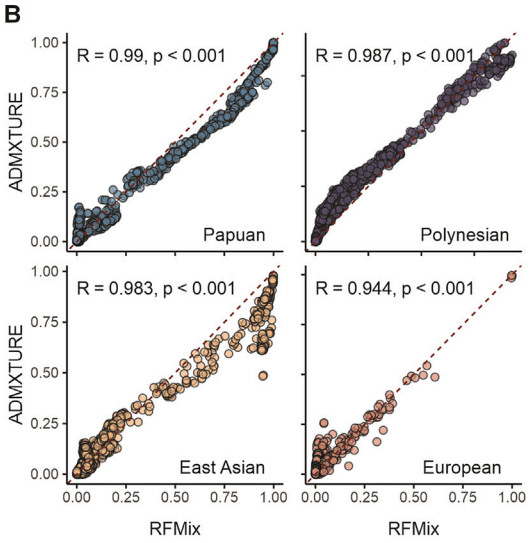

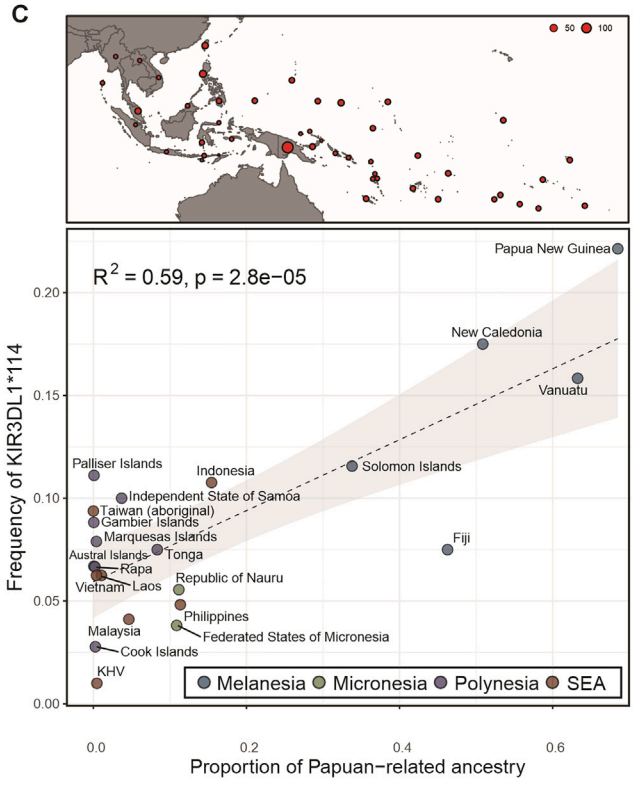

D

Ancestry (%)	KIR3DL1 allele		
	*114	*01502	*00501
Papuan	92.9%	14.0%	40.0%
East Asian	5.4%	58.1%	10.0%
Polynesian	1.8%	32.6%	30.0%
European	0.0%	1.2%	20.0%
N haplotypes	56	86	10

E

	W	D	Z
A*24:02	0.14	1.50
A*34:01	-0.38	-5.17
A*11:01	0.49	7.61

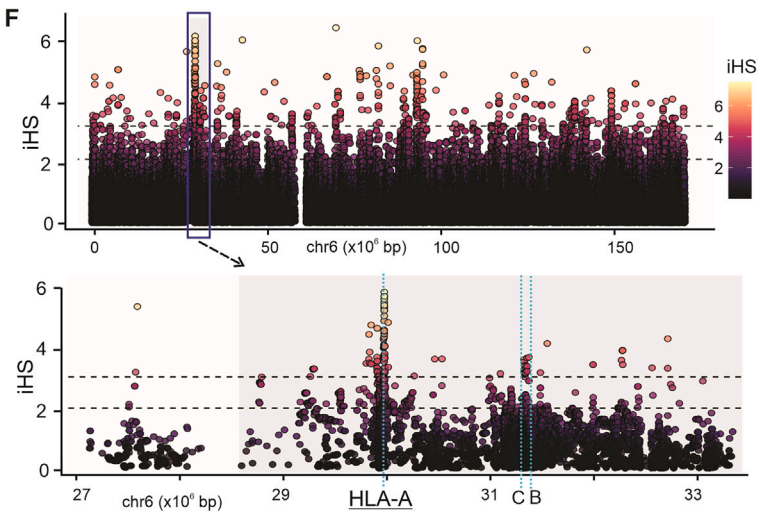

(legend on next page)

Figure S2. Identifying distribution and ancestry of KIR3DL1*114 and HLA-A*24:02, related to Figure 2

(A) Global ancestry proportions estimated using ADMIXTURE at K = 5 from SNP array data of the Oceanian and 1000G merged dataset. The major mode of ten independent runs is shown. Each vertical bar represents an individual. These global ancestry proportions were used to identify individuals to be used in the reference panel for the local ancestry inference using RFMIX.

(B) Quality control of the local ancestry analyses performed with RFMIX, showing the correlation between global ancestry proportions inferred from ADMIXTURE K = 5 and RFMIX. The high correlations indicate that RFMIX inference does not show a systemic bias in any of the ancestry panels. The results from RFMIX were used to identify the genetic ancestry of the *KIR3DL1*114*, **005-lineage*, and **015-lineage* haplotypes in our dataset.

(C) Correlation of genome-wide proportion of Papuan-related ancestry with frequency of *KIR3DL1*114*. Top: shows the populations represented by the OGVP. Each dot represents a population, with diameter corresponding to sample size. Bottom: Papuan-related ancestry for each population studies represents the mean genome-wide ancestry inferred from RFMix. Each dot represents a population group colored by region. SEA, Southeast Asia.

(D) Shows the number of *KIR3DL1*114*, **01502*, or **00501* carrying haplotypes having either Papuan, East Asian, Polynesian, or European Ancestry, as described in (B).

(E) Results of Z and D tests for Denisovan introgression of *HLA-A*24:02*, **34:01*, and **11:01*. An *HLA-A*11* sequence was identified previously to be present in the Denisovan genome.[35]

(F) Manhattan plot showing the positive iHS scores (representing selection on the derived alleles) performed on the *HLA-A*24:02* homozygous and heterozygous Papuans from SGDP.[95] Dashed lines represent top 1% and 5% iHS score thresholds.

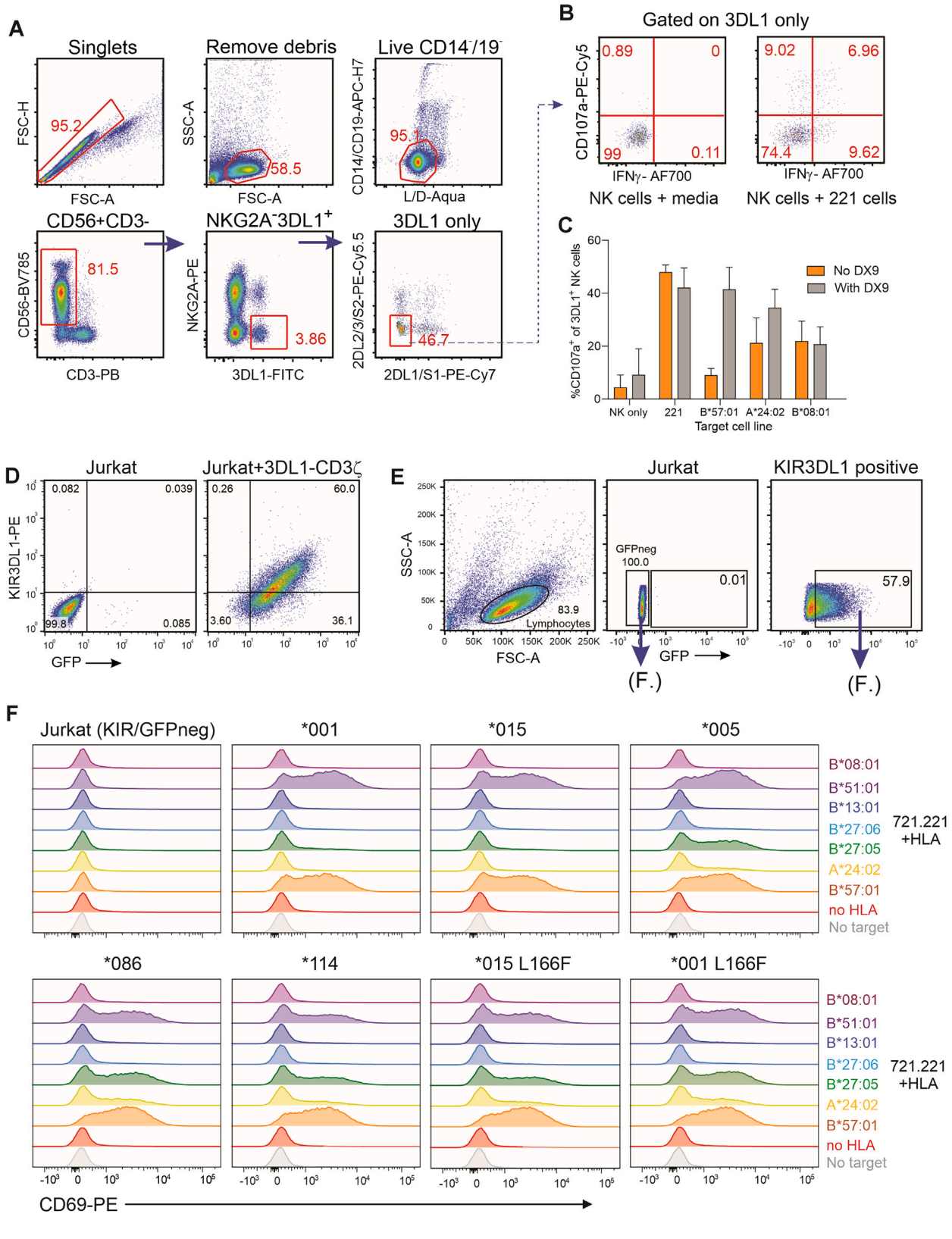

(legend on next page)

Figure S3. Flow cytometry gating strategies and controls for *ex vivo* and IL-2 expanded KIR3DL1$^+$ NK cell inhibition assays, related to Figure 3

(A) Flow cytometry gating strategy used to identify *ex vivo* single positive KIR3DL1$^+$ NK cells following incubation with target cells. (Left to right, top to bottom) Purified NK cells were first identified by their forward and side scatter, single cells were selected, and debris removed. Dead cells and those expressing CD14 or CD19 were excluded before gating on CD3$^-$ CD56$^+$ cells (NK cells). NK cells expressing KIR3DL1 but not NKG2A were next selected, and KIR3DL1$^+$ NK cells co-expressing KIR2DL1/S1 or KIR2DL2/3/S2 were excluded.

(B) Production of IFN-γ and CD107a by single positive KIR3DL1$^+$ NK cells alone or with targets was then assessed.

(C) Shows the results of NK cell experiments from two donors, with and without KIR3DL1 blocking. KIR3DL1$^+$ NK cells were sorted and expanded, then incubated with HLA-expressing target cells in the presence (gray) and absence (orange) of 10 μg/mL DX9 antibody. The resulting expression of CD107a was assessed using flow cytometry (A and B).

(D) Jurkat cells were transduced with KIR3DL1 allotypes fused to the intracellular domain of CD3ζ.

(E) GFP and KIR3DL1 expression on transduced Jurkat cells were assessed via flow cytometry, staining with anti-KIR3DL1/2-PE (clone 5.133: Miltenyi Biotec).

(F) Representative plots showing GFP expression and CD69 upregulation on reporter cells following 8 h incubation with a panel of HLA-transfected 721.221 target cells. Cells were stained with anti-CD69-PE and gated on GFP+ cells (untransfected cells on GFP negative cells), with the percentage of CD69+ cells taken as those with expression above that seen with no targets.

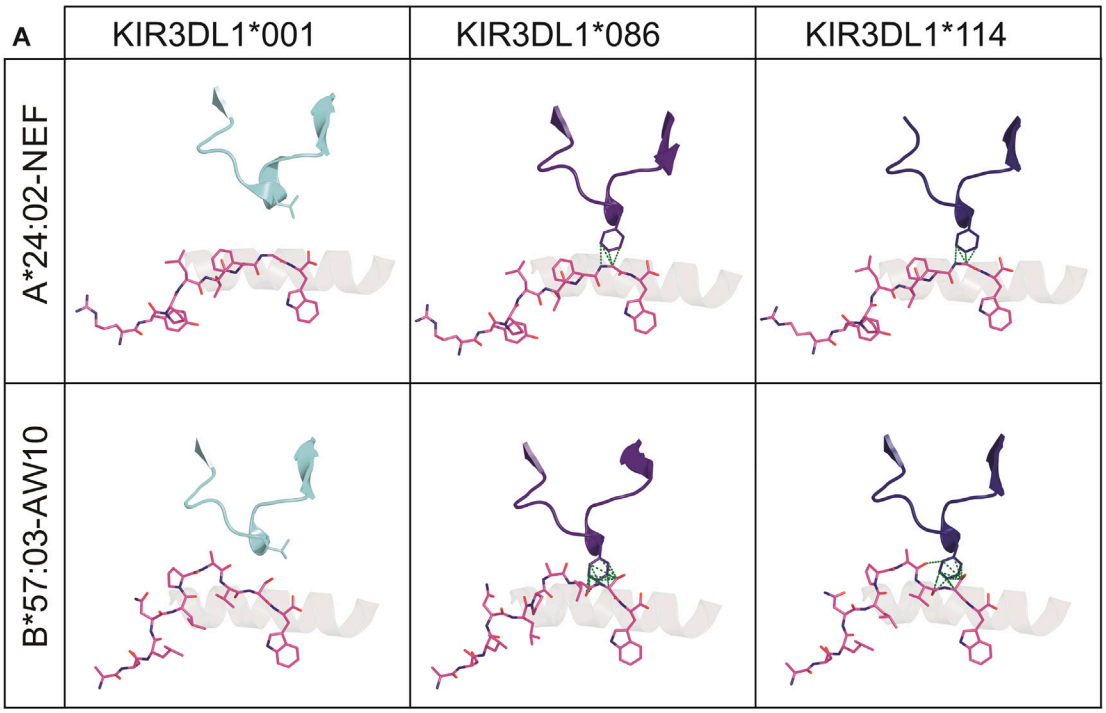

B Interactions with HLA molecule

Allotype	Interaction	KIR3DL1	HLA-A*24:02	Distance (Å)
*114	VDW	PHE166 [CD1]	GLU76 [CG]	3.45
		PHE166 [CD1]	GLU76 [OE1]	3.94
		PHE166 [CE1]	GLU76 [CG]	3.67
		PHE166 [CE1]	GLU76 [OE1]	3.74
		PHE166 [CE1]	ILE80 [CD1]	3.51
		PHE166 [CE1]	ILE80 [CG1]	3.63
		PHE166 [CE2]	ILE80 [CD1]	3.88
		PHE166 [CZ]	ILE80 [CG1]	3.43
		PHE166 [CZ]	ILE80 [CD1]	3.41
*001	VDW	LEU166 [CD2]	ILE80 [CD1]	3.92

C. Interactions with presented peptide

Allotype	Interaction	KIR3DL1	TW9	Distance (Å)
*114	H-Bonds	TYR200 [OH]	ASN8 [ND2]	3.75
		GLU282 [OE1]	ASN8 [ND2]	2.82
		GLU282 [OE2]	ARG7 [NH2]	3.49
	VDW	PHE166 [CB]	ASN8 [CG]	3.91
		PHE166 [CB]	ASN8 [OD1]	3.9
		PHE166 [CD2]	ASN8 [OD2]	3.87
*001	H-Bonds	Not present		
	VDW	LEU166 [CB]	ASN8 [OD1]	3.97
		LEU166 [CD2]	ASN8 [CB]	3.75

D Interactions with presented peptide

vdw Interactions	KIR3DL1*114 PHE 166	Peptide	Distance (Å)
NEF	CE1	GLY 7 (N)	3.93
	CE1	GLY 7 (CA)	3.64
	CE2	GLY 7 (CA)	3.77
	C2	GLY 7 (CA)	3.40
AW10	CD1	ALA 7 (O)	3.71
	CE1	VAL 8 (C)	3.78
	CE1	VAL 8 (O)	3.42
	C2	VAL 8 (O)	3.60
	CE1	SER 9 (CA)	3.87
	C2	SER 9 (CA)	3.73
	C2	SER 9 (CB)	3.60
	CG	SER 9 (CB)	3.54
	CD1	SER 9 (CB)	3.67
	CD2	SER 9 (CB)	3.41
	CE1	SER 9 (CB)	3.71
	CE2	SER 9 (CB)	3.45

Figure S4. Contact points of KIR3DL1 with HLA-peptide complexes, related to Figure 4

(A) Compares contact points of KIR3DL1 residue 166 with P8 from HLA-A*24:02-TW9 or B*57:03-AW10, across KIR3DL1 allotypes *001, *086, and *114.

(B and C) Shown are van der Waals (vdw) and hydrogen bonds (H-bonds) identified through crystallography of KIR3DL1*114 or *001 with HLA-A*24:02-TW9 complex. (B) Interactions of KIR3DL1 with HLA molecule. (C) Interactions of KIR3DL1 with TW9 peptide.

(D) Lists the vdw interactions between Phe-166 of KIR3DL1*114 and the peptide residues.

A

HLA	Peptide	Sequence	Organism	Antigen
HLA-A*24:02	TW9 549-557	TYQWIIRNW	Influenza A virus	Polymerase basic protein 2
	FF10 496-505	FYRYGFVANF		RNA-directed RNA polymerase catalytic subunit
	RF8 498-505	RYGFVANF		RNA-directed RNA polymerase catalytic subunit
	NEF 134-141	RYPLTFGW	HIV-1	Nef
HLA-B*57:03	AW10 850-859	ASLNLPAVSW	Homo sapiens	Catenin
HLA-C*05:01	SAE 67-75	SAEPVPLQL	HIV-1	Rev

B

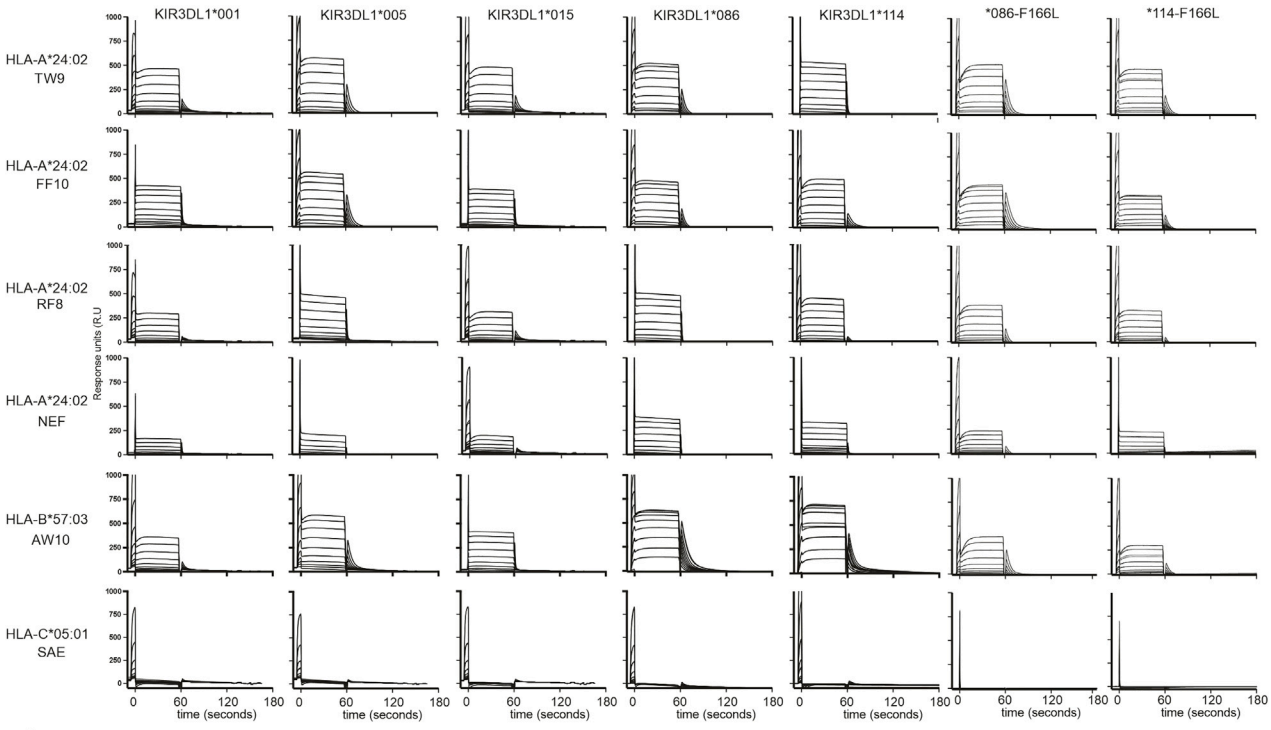

C

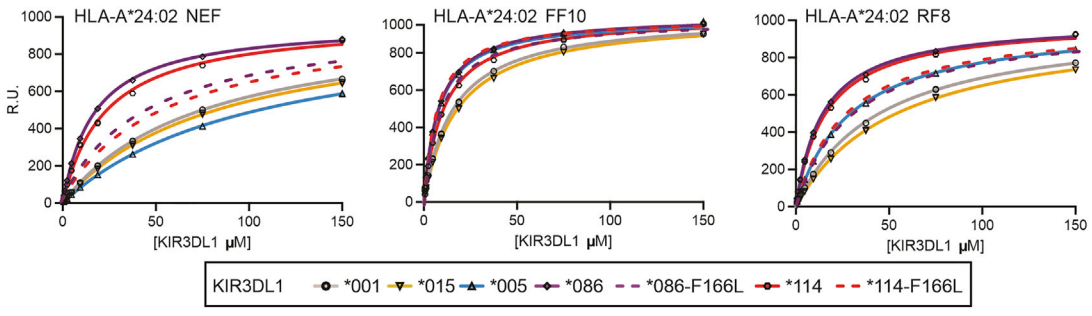

D

HLA-peptide	KIR3DL1*001	KIR3DL1*005	KIR3DL1*015	KIR3DL1*086	*086-F166L	KIR3DL1*114	*114-F166L
A*24:02 TW9	34.65 ± 0.14	18.07 ± 1.20	36.61 ± 2.43	8.88 ± 0.04	18.97 ± 1.95	10.44 ± 0.75	20.06 ± 2.8
A*24:02 FF10	15.94 ± 0.99	7.94 ± 0.28	18.07 ± 0.54	8.33 ± 0.03	9.14 ± 2.06	10.61 ± 0.72	6.67 ± 0.06
A*24:02 RF8	44.89 ± 3.25	29.28 ± 1.08	53.83 ± 1.08	15.28 ± 0.13	31.21 ± 4.81	15.93 ± 0.91	27.08 ± 0.13
A*24:02 NEF	75.01 ± 0.74	104.52 ± 10.1	82.17 ± 7.07	18.06 ± 0.07	45.07 ± 1.37	24.95 ± 2.53	53.27 ± 4.25
B*57:03 AW10	50.87 ± 0.35	42.90 ± 1.07	62.36 ± 1.03	1.99 ± 0.01	35.72 ± 0.05	2.07 ± 0.03	31.37 ± 3.93
C*05:01 SAE	N.B	N.B	N.B	N.B	N.B	N.B	N.B

(legend on next page)

Figure S5. Surface plasmon resonance: Peptides and data, related to Figure 5

(A) Sequence and origin of peptides used for HLA class I/peptide complexes. HLA-C*05:01-SAE is used as a negative control, which does not bind KIR3DL1.[24]

(B) Sensorgrams of KIR3DL1 allotypes (*001, *005, *015, *086, and *114, and mutations *086-F166L, *114-F166L) binding to refolded HLA-peptide complexes. Experiments were performed in duplicate, and one replicate is shown.

(C) Affinity curves of KIR3DL1 allotype binding to immobilized HLA-peptide complexes. R.U., response units.

(D) Steady-state K_D for interactions of KIR3DL1 allotypes with HLA-peptide complexes. N.B., no binding (no detectable interaction). Data are derived from two independent experiments.